Homeostatic structural plasticity leads to the formation of memory engrams through synaptic rewiring in recurrent networks

Júlia V. Gallinaro*[1], Nebojša Gašparović*[1], & Stefan Rotter[1]

March 27, 2020

* These authors contributed equally to this work

[1] Bernstein Center Freiburg & Faculty of Biology, University of Freiburg, Freiburg im Breisgau, Germany

Abstract

Brain networks store new memories using functional and structural synaptic plasticity. Memory formation is generally attributed to Hebbian plasticity, while homeostatic plasticity is thought to have an ancillary role in stabilizing network dynamics. Here we report that homeostatic plasticity alone can also lead to the formation of stable memories. We analyze this phenomenon using a new theory of network remodeling, combined with numerical simulations of recurrent spiking neural networks that exhibit structural plasticity based on firing rate homeostasis. These networks are able to store repeatedly presented patterns and recall them upon the presentation of incomplete cues. Storing is fast, governed by the homeostatic drift. In contrast, forgetting is slow, driven by a diffusion process. Joint stimulation of neurons induces the growth of associative connections between them, leading to the formation of memory engrams. In conclusion, homeostatic structural plasticity induces a specific type of "silent memories", different from conventional attractor states.

1 Introduction

Memories are formed in the brain using cell assemblies that emerge through coordinated synaptic plasticity. Cell assemblies with strong enough recurrent connections lead to bi-stable firing rates, which allows a network to encode memories as dynamic attractor states. In most theoretical models of cell assembly formation, the assemblies are generated by strengthening already existing synaptic contacts using appropriate synaptic learning rules [30, 46]. It was shown that attractor networks can also emerge through the creation of neuronal clusters with increased connectivity among neurons, leaving the weights of individual synaptic contacts unchanged [29].

The creation of clusters through changes in connectivity between cells would require synaptic rewiring, or structural plasticity. Structural plasticity has been frequently reported in different areas of the brain, and sprouting and pruning of synaptic contacts was found to be often activity-dependent [22, 31]. Sustained turnover of synapses, however, poses a severe challenge to the idea of memories being stored in synaptic connections [33]. Recent theoretical work has attempted to address the question, how stable assemblies can be maintained despite ongoing synaptic rewiring [10, 11].

The formation of neuronal assemblies, or clusters, is traditionally attributed to Hebbian plasticity, driven by the

correlation between pre- and postsynaptic neuronal activity on a certain time scale. For a typical Hebbian rule, a positive correlation in activity leads to an increase in synaptic weight, which in turn increases the correlation between neuronal firing. This positive feedback cycle can result in unbounded growth, runaway activity and dynamic instability of the network, if additional regulatory mechanisms are lacking. In fact, neuronal networks of the brain are known to employ homeostatic control mechanisms that regulate neuronal activity [43], and possibly even stabilize the firing rate of individual neurons at specific target levels [19, 40]. However, even though homeostatic mechanisms have been reported in experiments to operate on a range of different time scales, they seem to be too slow to trap the instabilities caused by Hebbian learning rules [47]. All things considered, what are the exact roles of Hebbian and homeostatic plasticity, and how these different processes interact to form cell assemblies in a robust and stable way, remains to be elucidated [25].

Concerning the interplay between Hebbian and homeostatic plasticity, we have recently demonstrated by simulations that homeostatic structural plasticity alone can lead to the formation of assemblies of strongly interconnected neurons, and that this process of memory formation has associative properties [12]. Moreover, we found that varying the strength of the stimulation and the fraction of stimulated neurons in combination with repetitive protocols can lead to even stronger assemblies [32]. In both papers, we used a structural plasticity model based on firing rate homeostasis, which had been used before to study synaptic rewiring linked with neurogenesis [6, 7], and the role of structural plasticity after focal stroke [3, 5] and after retinal lesion [2]. This model has also been used to study the emergence of criticality in developing networks [39] and other topological aspects of plastic networks [4]. The memories formed in networks of this type, however, are of a different nature than the ones found in attractor networks. Firstly, structural plasticity operates at a slower time scale than functional plasticity, leading to slower assembly formation. Secondly, the formed assemblies represent a form of silent memory that is not in every moment reflected by neuronal activity.

The long-standing discussion about memory engrams in the brain has been revived recently. Researchers were able to identify and manipulate engrams [24], and to allocate memories to specific neurons during classical conditioning tasks [23]. These authors have also emphasized that an engram is not yet a memory, but the physical substrate of a potential memory in the brain [24]. Similar to the idea of a memory trace, it should provide the necessary conditions for a retrievable memory to emerge. Normally, the process of engram formation is thought to involve the strengthening of already existing synaptic connections. Here, we propose that new engrams could also be formed by an increase in synaptic connectivity and the formation of neuronal clusters.

Among other things, we perform numerical simulations of a classical conditioning task in a recurrent network with structural plasticity based on firing rate homeostasis. We show that the cell assemblies formed share all characteristics of a memory engram. We further explore the properties of the formed engrams and develop a mean-field theory to explain the mechanisms of memory formation with homeostatic structural plasticity. We show that these networks are able to effectively store repeatedly presented patterns, and that the formed engrams implement a special type of silent memory, which normally exists in a quiescent state and can be successfully retrieved based on incomplete cues.

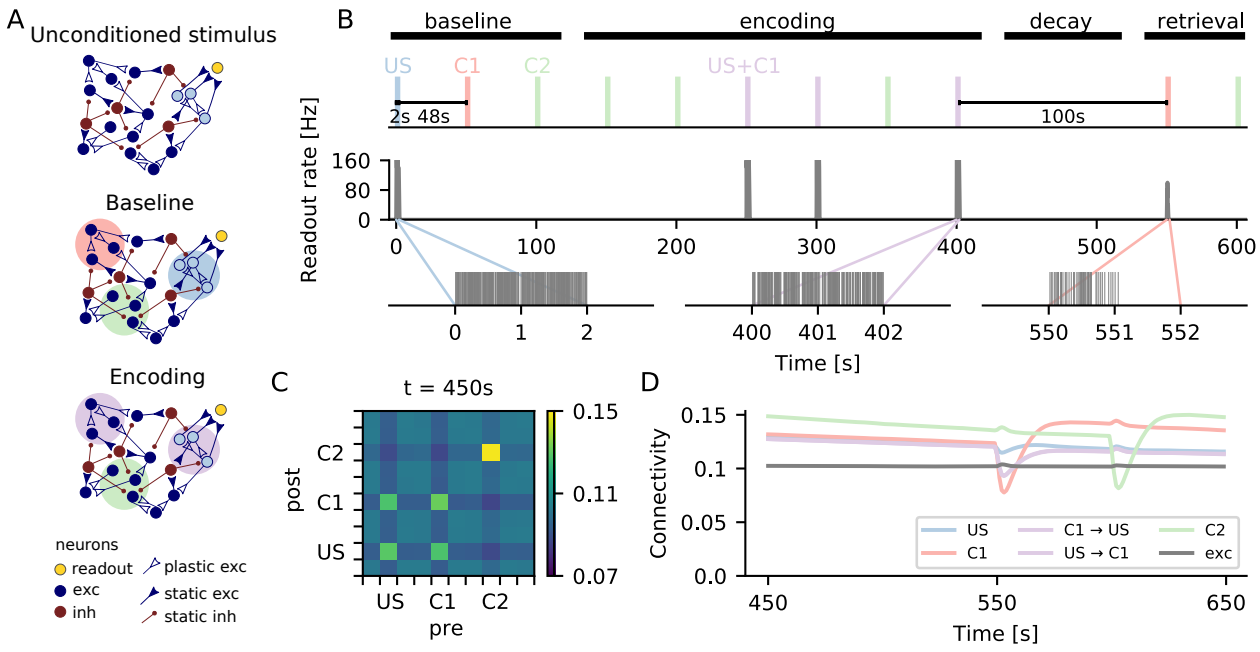

Figure 1: Formation of memory engrams in a neuronal network with homeostatic structural plasticity. (A) In a classical conditioning scenario, a conditioned stimulus C1 is paired with an unconditioned stimulus US ("encoding"), and another conditioned stimulus C2 is presented alone. (B) Before the paired stimulation ("baseline"), the readout neuron responds strongly only upon direct stimulation of the neuronal ensemble corresponding to the US. After the paired stimulation ("retrieval"), however, a presentation of C1 alone triggers a strong response of the readout neuron. This is not the case for a presentation of C2 alone. *Top:* stimulation and retrieval of the conditioning protocol; *middle:* firing rate of the readout neuron; *bottom:* spike train of the readout neuron during the baseline (left), encoding (middle) and retrieval (right) phase. (C) After encoding, the connectivity matrix indicates that engrams have formed, and we find enhanced connectivity within all three ensembles as a consequence of repeated stimulation. Bidirectional inter-connectivity across different engrams, however, is only observed for the pair C1 and US, which experienced paired stimulation. (D) The connectivity dynamics shows that engram identity are strengthened with each stimulus presentation, and that they decay during unspecific external stimulation.

2 Results

2.1 Formation of memory engrams by homeostatic structural plasticity

We simulate a classical conditioning paradigm using a recurrent network. The network is composed of excitatory and inhibitory leaky integrate-and-fire neurons, and the excitatory-to-excitatory connections are subject to structural plasticity regulated by firing rate homeostasis. Three different non-overlapping neuronal ensembles are sampled randomly from the network. The various stimuli considered here are conceived as increased external input to one of the specific ensembles, or combinations thereof. As the stimuli are arranged exactly as in behavioral experiments, we also adopt their terminology "unconditioned stimulus" (US) and "conditioned stimulus" (C1 and C2). The unconditioned response (UR) is conceived as the activity of a single readout neuron, which receives input from the ensemble of excitatory neurons associated with the US (Figure 1A, top).

Figure 1B illustrates the protocol of the conditioning experiment simulated here. During a baseline period, the engrams representing US, C1 and C2 are stimulated one after the other. In this phase, the activity of the US

ensemble is high only upon direct stimulation (Figure 1B, middle). The baseline period is followed by an encoding period, in which C1 is paired with US, while C2 is always presented in isolation. Simultaneous stimulation of neurons in a recurrent network with homeostatic structural plasticity can lead to the formation of reinforced ensembles [12], which are strengthened by repetitive stimulation [32]. After the encoding period, each of the three neuronal ensembles has increased within-ensemble connectivity, as compared to baseline. Memory traces, or engrams, have formed (Figure 1C). Moreover, the US and C1 engrams also have higher bidirectional across-ensemble connectivity, representing an association between their corresponding memories.

Between encoding and retrieval, memory traces remain in a dormant state. Due to the homeostatic nature of network remodeling, the spontaneous activity after encoding is very similar to the activity before encoding, but specific rewiring of input and output connections have lead to the formation of structural engrams. It turns out that these "silent memories" are quite persistent, as "forgetting" is much slower than "learning" them (see below for a detailed analysis of this phenomenon). Any silent memory can be retrieved with a cue, or in our case, by presentation of the conditioned stimulus. Stimulation of C1 alone, but not of C2 alone, triggers a conditioned response (Figure 1B) that is similar to the unconditioned response. Inevitably, stimulation of C1 and C2 during recall briefly destabilizes the corresponding cell assemblies, as homeostatic plasticity is still ongoing. The corresponding engrams then go through a reconsolidation period, during which the within-assembly connectivity grows even higher than before retrieval (Figure 1D, red and green). As a consequence, stored memories get stronger with each recall. Interestingly, as in our case the retrieval involves stimulation of either C1 or C2 alone, the connectivity between the US and C1 engrams decreases a bit after the recall (Figure 1D, purple).

Memories and associations are formed by changes in synaptic wiring, triggered by neuronal activity during the encoding period. They persist in a dormant state and can be reactivated by a retrieval cue that reflects the activity experienced during encoding. This setting exactly characterizes a memory engram [24]. In the following sections, we will analyze the process of memory formation further and explore the nature of the formed engrams in more detail.

2.2 Engrams represent silent memories, not attractors

Learned engrams have a subtle influence on network activity. For a demonstration, we first grow a network under the influence of homeostatic structural plasticity (see 4.10.1). We then randomly select an ensemble E_1 of excitatory neurons and stimulate it repeatedly. Each stimulation cycle is comprised of a period of 150 s increased input to E_1 and another 150 s relaxation period with no extra input. After 8 such stimulation cycles, the within-engram connectivity has increased to $C_{E_1E_1} \approx 0.21$. At this point, the spontaneous activity of the network exhibits no apparent difference to the activity before engram encoding (Figure 2A). Due to the homeostatic nature of structural plasticity, neurons fire on average at their target rate, even though massive rewiring has led to higher within-engram connectivity. Looking closer, though, reveals a conspicuous change in the second-order properties of neuronal ensemble activity. We quantify this phenomenon using the overlap m^μ (see 4.10.8 for a detailed explanation of the concept). Figure 2B depicts the time-dependent overlap of spontaneous network activity with the engram E_1 (m^{E_1}). It also shows the overlap with 10 different random ensembles x (m^x), which are of the same size as E_1 but have no neurons in common with it. The variance of m^{E_1} is slightly larger than that of m^x (Figure 2C). This indicates that the increased connectivity also increases the tendency of neurons belonging to the same learned engram to synchronize their activity and increase their correlation, in comparison to other

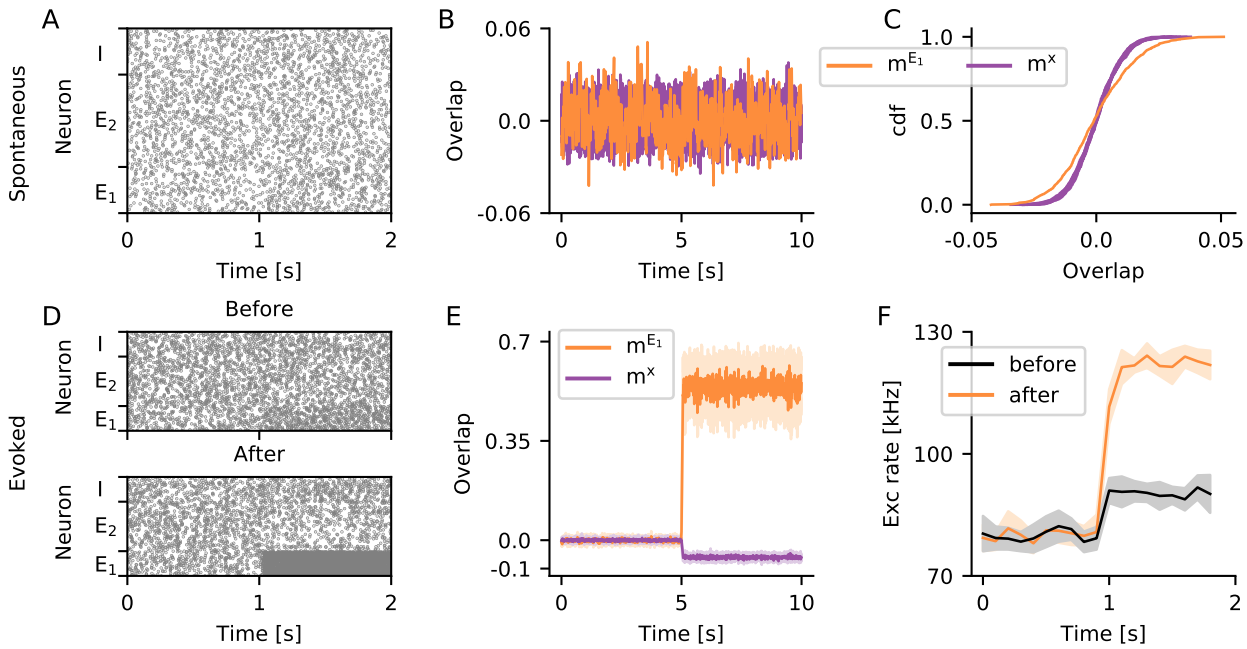

Figure 2: Silent memory based on structural engrams. (A–C) The spontaneous activity of neurons belonging to the engram E_1 is hardly distinguishable from the activity of the rest of the network. (A) Raster plot showing the spontaneous activity of 50 neurons randomly selected from E_1, 100 neurons randomly selected from E_2 but not belonging to E_1, and 50 neurons randomly selected from the pool I of inhibitory neurons. (B) Overlap of spontaneous network activity with the learned engram E_1 (m^{E_1}, orange) and for 10 different random ensembles x disjoint with E_1 (m^x, purple). (C) Cumulative distribution of m^μ shown in (B). (D–F) The activity evoked upon stimulation of E_1 is higher, if the within-engram connectivity is large enough ($C_{E_1E_1} > 0.1$) as a consequence of learning. (D) Same as (A) for evoked activity, the stimulation starts at $t = 1\,\mathrm{s}$. The neurons belonging to engram E_1 are stimulated before (top, $C_{E_1E_1} \approx 0.1$) and after (bottom, $C_{E_1E_1} \approx 0.21$) engram encoding. (E) Overlap with the learned engram (m^{E_1}, orange) and with random ensembles (m^x, purple) during specific stimulation of engram E_1. (F) Population rate of all excitatory neurons during stimulation of E_1 before (black) and after (orange) engram encoding. (E, F) Solid line and shading depict mean and standard deviation across 10 independent simulation runs, respectively. In all panels, the bin size for calculating overlaps are 10 ms, and the bin size for calculating population rates is 100 ms.

pairs of neurons. An increase in pairwise correlations within the engram also leads to increased fluctuations of the population activity [26], which also affects population measures such as the overlap used here.

During specific stimulation, the differences between the evoked activity of learned engrams and random ensembles are more pronounced. Figure 2D shows raster plots of network activity during stimulation of E_1 before and after the engram has been encoded. The high recurrent connectivity within the E_1 assembly after encoding amplifies the effect of stimulation, leading to much higher firing rates of E_1 neurons. This effect can even be seen in the population activity of all excitatory neurons in the network (Figure 2F). During stimulation, the increase in firing rate of engram neurons is accompanied by a suppression of activity of all other excitatory neurons not belonging to the engram. This is what underlies the conspicuous decrease in the overlap m^x with random ensembles x during stimulation (Figure 2E).

How does all this affect the strength of a memory? To answer this question, we looked into evoked activity

at different points in time during stimulation. The within-engram connectivity increases with every stimulation cycle (Figure 3A), and so does the population activity of excitatory neurons during stimulation (Figure 3B). The in-degree of excitatory neurons, in contrast, is kept at a fixed level by the homeostatic controller, even after engram encoding (Figure 4C). This behavior is well captured by a simple mean-field firing rate model (grey line in Figure 3B), in which the within-engram connectivity is varied and all the remaining excitatory connections are adjusted to maintain a fixed in-degree of excitatory neurons.

Engrams exhibit pattern completion to a degree that depends on the strength of the memory. We quantitatively assess pattern completion by measuring how the overlap of network activity with the engram, m^{E_1}, depends on partial stimulation. For an unstructured random network, m^{E_1} increases at a certain rate with the fraction of stimulated neurons (Figure 3C, black line). We speak of "pattern completion", if m^{E_1} increases at a larger rate with size than in an unstructured random network. Figure 3C demonstrates very clearly that the degree of pattern completion associated with a specific engram increases monotonically with the strength of the memory, that is, with the within-engram connectivity.

The difference in evoked activity between learned engrams and random ensembles of the same size can be taken as evidence for the existence of a stored memory. To demonstrate the potential of this idea, we employ a simple readout neuron for this task (Figure 3D). This neuron has the same properties as any other neuron in the network, and it receives input from a random sample comprising a certain fraction (here 9 %) of all excitatory and the same fraction of all inhibitory neurons in the network. We encode two engrams in the same network, one being slightly stronger ($C_{E_1E_1} \approx 0.19$, green) than the other one ($C_{E_2E_2} \approx 0.18$, orange). We record the firing of the readout neuron during spontaneous activity, during specific stimulation of the engrams, and during stimulation of random ensembles. Figure 3E shows a raster plot of the activity of 10 different readout neurons, each of them sampling a different subset of the network. With the parameters considered here, the activity of a readout neuron is generally very low, except when a learned memory engram is stimulated. Due to the gradual increase in population activity with memory strength (Figure 3B), readout neurons respond with higher rates upon the stimulation of stronger engrams (green).

Homeostatic structural plasticity enables memories based on neuronal ensembles with increased within-ensemble connectivity, or engrams. Memories are acquired quickly and can persist for a long time. Moreover, the specific network configuration considered here admits a gradual response to the stimulation of an engram according to the strength of the memory. Mathematically speaking, the engram connectivity lies on a line attractor which turns into a slow manifold, if fluctuations are taken into consideration. This configuration allows the network to simultaneously learn to recognize a stimulus ("Does the current stimulation corresponds to a known memory?") and to assess its confidence of the recognition ("How strong is the memory trace of this pattern?"). Such behavior would be absolutely impossible in a system that relies on bistable firing rates (attractors) to define engrams. Details of our analysis will be explained later in section 2.4.

2.3 The mechanism of engram formation

We have shown how homeostatic structural plasticity creates and maintains the memory engrams, and we will now further elucidate the mechanisms underlying this process. We consider a minimal stimulation protocol [12] to study the encoding process for a single engram E_1. We perform numerical simulations and develop a dynamical

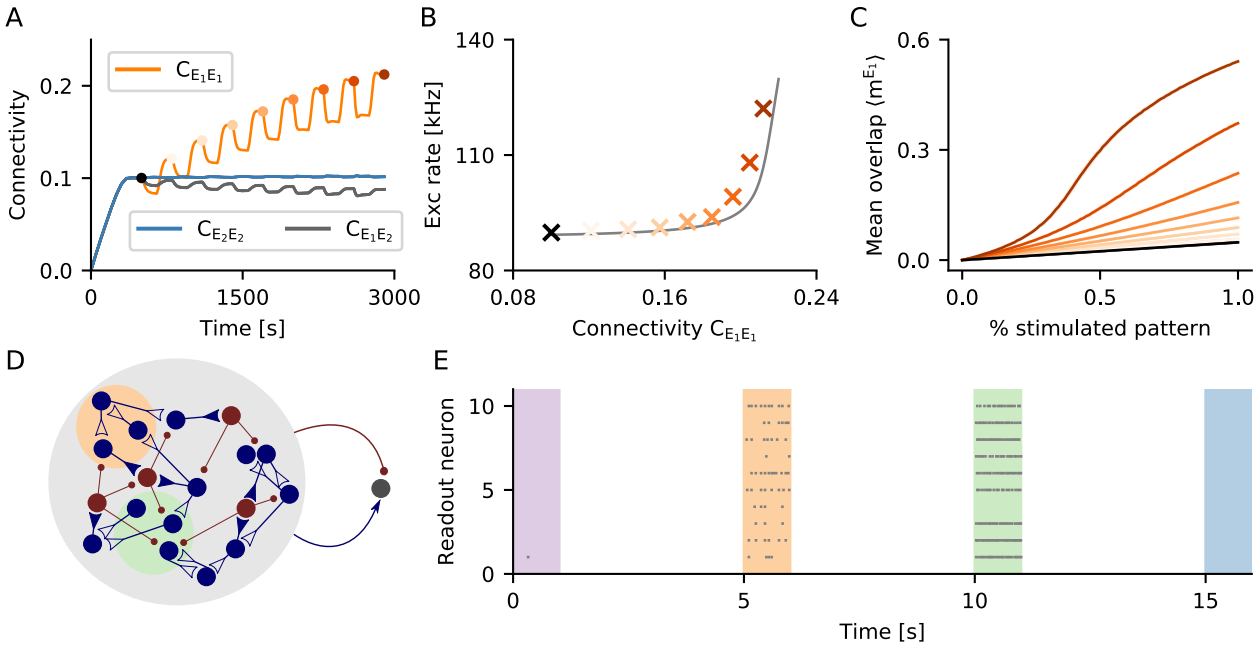

Figure 3: Evoked activity depends on the strength of memories. (A) Starting from a random network grown under the influence of unstructured stimulation (black dot), we repeatedly stimulate the same ensemble of excitatory neurons E_1 to eventually form an engram. Multiple stimulation cycles increase the recurrent connectivity within the engram. (B) Population activity of all excitatory neurons upon stimulation of E_1, for different levels of engram connectivity $C_{E_1E_1}$. Crosses depict the population rate observed in a simulation. Colors indicate engram connectivity $C_{E_1E_1}$, matching the colors used in panels (A) and (C). The grey line outlines the expectation from a simple mean-field theory. (C) Time-averaged overlap $\langle m^{E_1} \rangle$, for different fractions of E_1 being stimulated. The recurrent nature of memory engrams enables them to perform pattern completion. The degree of pattern completion depends monotonically on engram strength. (D) Two engrams (orange and green) are encoded in a network. Both engrams have a different strength with regard to their within-engram connectivity (green stronger than orange). A simple readout neuron receives input from a random sample comprising 9 % of all excitatory and 9 % of all inhibitory neurons in the network. (E) Raster plot for the activity of 10 different readout neurons during the stimulation of learned engrams and random ensembles, respectively. Readout neurons are active, when an encoded engram is stimulated (orange and green), and they generally respond with higher firing rates for the stronger engram (green). The activity of a readout neuron is low in absence of a stimulus (white), or upon stimulation of a random ensemble of neurons (purple and blue).

network theory to explain the emergence of associative (Hebbian) properties. In Figure 4, the results of numerical simulations are plotted together with the results of our theoretical analysis (see Section 4.6). Upon stimulation, the firing rate follows the typical homeostatic dynamics [44]. In the initial phase, the network stabilizes at the target rate (Figure 4A). Upon external stimulation, it transiently responds with a higher firing rate. With a certain delay, the rate is down-regulated to the set-point. When the stimulus is turned off, the network transiently responds with a lower firing rate, which is eventually up-regulated to the set-point again.

Firing rate homeostasis is based on the intracellular calcium concentration $\phi_i(t)$ of each neuron i (Figure 4D), which can be considered as a proxy for the firing rate of the neuron. In our simulations, it is obtained as a low-pass

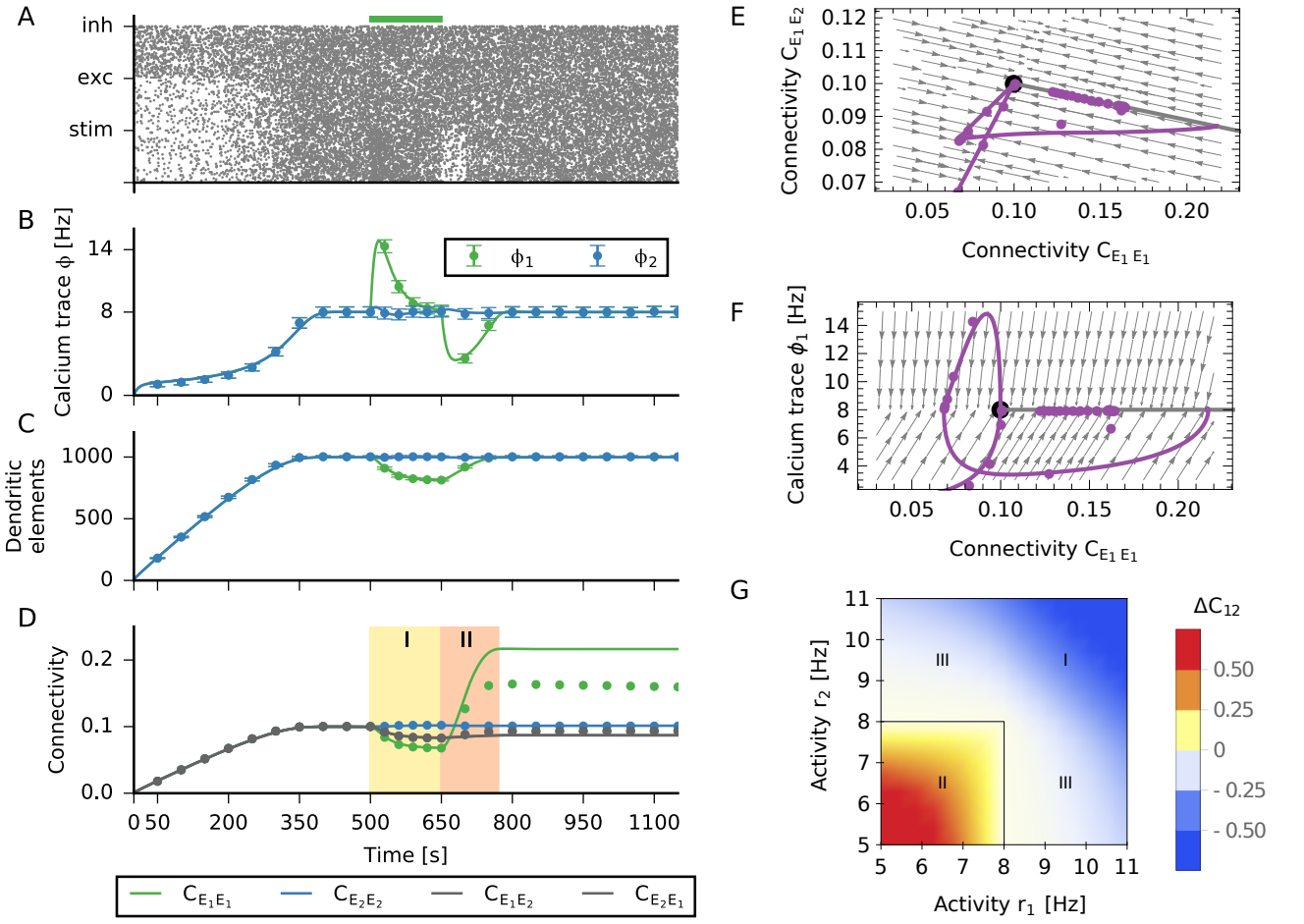

Figure 4: Hebbian properties emerge through interaction of selective input and homeostatic control. (A) The activity of the neuronal network is subject to homeostatic control. For increased external input, it transiently responds with a higher firing rate. With a certain delay, the rate is down-regulated to the imposed set-point. When the stimulus is turned off, the network transiently responds with a lower firing rate, which is eventually up-regulated to the set-point again. The activity is generally characterized by irregular and asynchronous spike trains. (B) It is assumed that the intracellular calcium concentration follows the spiking dynamics, according to a first-order low-pass characteristic. Dots correspond to numerical simulations of the system, and solid lines reflect theoretical predictions from a mean-field model of dynamic network remodeling. (C) Dendritic elements (building blocks of synapses) are generated until an in-degree of $K_{\text{in}} = 1\,000$ has been reached. It decreases during specific stimulation, but then recovers after the stimulus has been removed. (D) Synaptic connectivity closely follows the dynamics of dendritic elements until the recovery phase, when the recurrent connectivity within the stimulated group E_1 overshoots. (E, F) Phase space analysis of the activity. The purple lines represent projections of the full, high-dimensional dynamics to two-dimensional subspaces: (E) within-engram connectivity vs. across-ensemble connectivity and (F) within-engram connectivity vs. engram calcium trace. The dynamic flow is represented by the gray arrows. The steady state of the plastic network is characterized by a line attractor (thick gray line), defined by a fixed total in-degree and out-degree. The ensemble of stimulated neurons forms a stable engram, and the strength of the engram is encoded by its position on the line attractor. (G) The overshoot in connectivity can be explained as follows: After turning off the stimulus, neurons in the recently stimulated group are active below their target rate (set-point of the homeostatic controller), while other neurons are close to their equilibrium activity. This leads to a faster creation of recurrent connectivity within the stimulated group, as compared to connections involving neurons outside it.

filtered version of the spike train $S_i(t)$ of the same neuron

$$\tau_{\mathrm{Ca}}\dot{\phi}_i(t) = (S_i(t) - \phi_i(t)), \tag{1}$$

with time constant τ_{Ca}. Each excitatory neuron i uses its own calcium trace $\phi_i(t)$ to control its number of synaptic elements. Deviations of the instantaneous firing rate (calcium concentration) $\phi_i(t)$ from the target rate ν_i (the set-point) trigger either creation or deletion of elements according to

$$\beta_d\dot{d}_i(t) = \nu_i - \phi_i(t), \qquad \beta_a\dot{a}_i(t) = \nu_i - \phi_i(t), \tag{2}$$

where $a_i(t)$ and $d_i(t)$ are the number of axonal and dendritic elements, respectively. The parameters β_a and β_d are the associated growth parameters (see Section 4.2 for more details).

During the initial growth phase, the number of elements increase to values corresponding to an in-degree $K^{\mathrm{in}} = \epsilon N$, which is the number of excitatory inputs to the neuron that are necessary to sustain firing at the target rate (Figure 4D). Upon stimulation (during the learning phase), the number of connections is down-regulated due to the transiently increased firing rate of neurons. After the stimulus is turned off, the activity returns to its set-point. During the growing and learning phases, connectivity closely follows the dynamics of synaptic elements (Figure 4D), and connectivity is proportional to the number of available synaptic elements (Figure 4D). After removal of the stimulus, however, in the reconsolidation phase, the recurrent connectivity within the stimulated group E_1 overshoots (Figure 4D), and the average connectivity in the network returns to baseline (Figure 4C). While recurrent connectivity $C_{E_1E_1}$ of the engram E_1 increases, both the connectivity to the rest of network $C_{E_2E_1}$ and from rest of the network $C_{E_1E_2}$ decrease, keeping the mean input to all neurons fixed. This indicates that although the network is globally subject to homeostatic control, local changes effectively exhibit associative features, as already pointed out in [12]. Our theoretical predictions generally match the simulations very well (Figure 4), with the exception that it predicts a larger overshoot. This discrepancy will only be resolved in Section 2.4.

Deriving a theoretical framework of network remodeling (see Section 4.3) for the algorithm suggested by [2] poses a great challenge due to the large number of variables of both continuous (firing rates, calcium trace) and discrete (spike times, number of elements, connectivity, rewiring step) nature. The dimensionality of the system was effectively reduced by using a mean-field approach, which conveniently aggregates discrete counting variables into continuous averages (see Section 4.4 and Section 4.6 for more details of derivation).

The number of newly created synaptic elements are denoted as free axonal $a^+(t)$ and free dendritic $d^+(t)$ elements, while the number of deleted elements is denoted by $a^-(t)$ and $d^-(t)$. Free axonal elements are paired with free dendritic elements in a completely random fashion to form synapses. The deletion of dendritic or axonal elements in neuron i automatically induces the deletion of incoming or outgoing synapses of that neuron, respectively. We derived a stochastic differential equation (Section 4.4) which describes the time evolution of connectivity $C_{ij}(t)$ from neuron j to neuron i

$$\frac{dC_{ij}(t)}{dt} = \underbrace{\frac{\rho'^{+}_{d_i}(t)\rho'^{+}_{a_j}(t)}{\rho(t)} - C_{ij}(t)\left(\frac{\rho^{-}_{d_i}(t)}{K^{in}_i(t)} + \frac{\rho^{-}_{a_j}(t)}{K^{out}_j(t)}\right)}_{\text{deterministic drift}} + \underbrace{\frac{dW_{\text{spike noise}}}{dt} + \frac{dW_{\text{structural noise}}}{dt}}_{\text{stochastic noise}}. \tag{3}$$

In this equation, $\rho^{\pm}_{a_i}(t)$, $\rho^{\pm}_{d_i}(t)$ is the rate of creation/deletion of the axonal and dendritic elements of neuron i, respectively, and $\rho(t)$ is the rate of creation of elements in the whole network. Note that ρ'^{+} is a corrected version

of ρ^+ (see Section 4.4 for details). The stochastic process described by Equation 3 decomposes into a deterministic drift process and a diffusive noise process. The noise process has two sources. The first derives from the stochastic nature of the spike trains, and the second is linked with the stochastic nature of axon-dendrite bonding. In this section, we ignore the noise and discuss only the deterministic part of the equation. This is equivalent to reducing the spiking dynamics to a firing rate model and, at the same time, coarse-grain the fine structure of connectivity.

Stable steady-state solutions of the system described by Equation 3 represent a hyperplane in the space of connectivity (see Equation 17 in Section 4.7). The solutions of Equation 3 are (random) network configurations with a fixed in-degree K_i^{in} and out-degree K_i^{out} such that $C^*_{i,j} \propto K_i^{\text{in}} K_j^{\text{out}}$. In the case of only one engram, the attractor reduces to a line (Figure 4E and F, gray line). This also explains how memories are stored in the network: When a group of neurons is repeatedly stimulated, the network each time diverges from the line attractor and takes a different path back during reconsolidation. The new position on the line encodes the strength of the memory $C_{E_1E_1}$. Furthermore, as the attractor is a skew hyperplane in the space of connectivity, the memory is distributed across the whole neural network, and not only in recurrent connections among stimulated neurons in E_1. As a reflection of this, other connectivity parameters ($C_{E_2E_2}$, $C_{E_1E_2}$, $C_{E_2E_1}$, cf. Figure 4D) are also slightly changed.

To understand why changes in recurrent connectivity $C_{E_1E_1}$ are associative, we note that the creation part of Equation 3 is actually an outer product of $\rho^+_{a_i}(t)$ and $\rho^+_{d_i}(t)$, similar to a pre-post pair in a typical Hebbian rule. The main difference to a classical Hebbian rule is that only neurons firing below their target rate are creating new synapses. The effective rule is depicted in Figure 4G. Only neurons with free axonal or dendritic elements, respectively, can form a new synapse, and those neurons are mostly the ones with low firing rates. The deletion part of Equation 3 depends linearly on $\rho^-_{a_i}(t)$ and $\rho^-_{d_i}(t)$, reducing to a simple multiplicative homeostasis. Upon excitatory stimulation, the homeostatic part is dominant and the number of synaptic elements decreases. After removal of the stimulus, the Hebbian part takes over, inducing a post-stimulation overshoot in connectivity. This leads to a peculiar dynamics of first decreasing connectivity and then overshooting, an important signature of this rule. We summarize this process in an effective rule

$$\Delta c_{ij} \quad \propto \quad \lambda \underbrace{\Delta I_i \Delta I_j}_{\text{effective Hebbian}} - \gamma_a \underbrace{c_{ij}(t)\Delta I_i}_{\text{dendritic homeostasis}} - \gamma_d \underbrace{c_{ij}(t)\Delta I_j}_{\text{axonal homeostasis}}, \tag{4}$$

where ΔI_i is the input perturbation of neuron i. The term $\Delta I_i \Delta I_j$ is explicitly Hebbian with regard to input perturbations. Equation 4 only holds, however, if the stimulus is presented for a long enough time such that the calcium concentration tracks the change in activity and connectivity drops.

2.4 Fluctuation-driven decay of engrams

The qualitative aspects of memory formation have been explored in Section 2.3. Now we investigate the process of memory maintenance. A noticeable discrepancy between theory and numerical simulations was pointed out in Figure 4D. The overshoot is exaggerated and memories last forever. We will now demonstrate that this discrepancy is resolved when we take the spiking nature of neurons into account (Section 4.5).

Neurons use discrete spike trains $S_i(t) = \sum_k \delta(t - t_k^i)$ for signaling, and we conceive them here as stochastic point processes. We found that Gamma processes (Section 4.5) can reproduce the first two moments of the spike train statistics of the simulated networks with sufficient precision. The homeostatic controller in our model uses the trace of the calcium concentration $\phi_i(t)$ as a proxy for the actual firing rate of the neuron. As the calcium trace

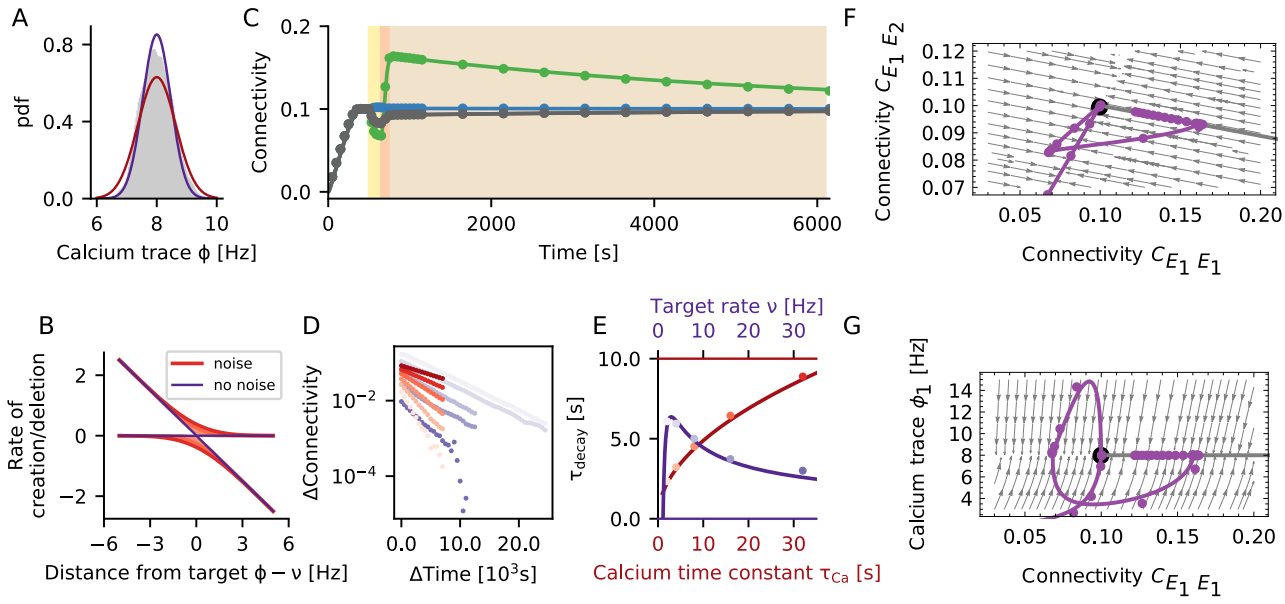

Figure 5: Noisy spiking induces fluctuations that lead to memory decay. (A) The gray histogram shows the distribution of calcium levels for a single neuron across 5 000 s of simulation. The colored lines result from modeling the spike train as a Poisson process (red) or a Gamma process (purple), respectively. (B) The rate of creation or deletion of synaptic elements depends on the difference between the actual firing rate from the target rate (set-point), for different levels of spiking noise. The negative gain (slope) of the homeostatic controller in presence of noise is transformed into two separate processes of creation and deletion of synaptic elements. In the presence of noise (red lines, darker colors correspond to stronger noise), even when the firing rate is on target, residual fluctuations in the calcium signal induce a constant rewiring of the network, corresponding to a diffusion process. (C) If noisy spiking and the associated diffusion is included into the model, predictions from a mean-field theory match the simulation results very well. This concerns the initial decay (yellow), the overshoot (red) and subsequent slow decay (brown). (D) Change in connectivity during the decay period (brown), for different values of the calcium time constant and the target rate. We generally observe exponential relaxation as a consequence of a constant rewiring rate. (E) Time constant of the diffusive decay as a function of the calcium time constant and the target rate. Lines show our predictions from theory, and dots represent the values extracted from numerical simulations of plastic networks. The decay time τ_{decay} increases with $\sqrt{\tau_{\text{Ca}}}$. The memory is generally more stable for small target rates ν, but collapses for very small rates. This predicts an optimum for low firing rates, at about 3 Hz. (F, G) Same phase diagrams as shown in Figures 4E and F, but taking noise into consideration. (F) The spiking noise compromises the stability of the line attractor, which turns into a slow manifold. (G) The relaxation to the high-entropy connectivity configuration during the decay phase is indeed confined to a constant firing rate manifold.

$\phi_i(t)$ is just a filtered version of the stochastic spike train $S_i(t)$, it is a stochastic process in its own respect. In Figure 5A we show the stationary distribution of the time-dependent calcium concentration $\phi_i(t)$. Apparently, a filtered Gamma process (purple line) provides a better fit to the simulated data than a filtered Poisson process (red line). The reason is that Gamma processes have an extra degree of freedom to match the irregularity of spike trains (coefficient of variation, here CV ≈ 0.7) as compared to Poisson processes (always CV $= 1$).

The homeostatic controller strives to stabilize $\phi_i(t)$ at a fixed target value ν, but $\phi_i(t)$ fluctuates (Figure 5A) due

to the random nature of the spiking. These fluctuations result in some degree of random creation and deletion of connections. Our theory (Section 4.5) reflects this aspect by an effective homeostatic function (Equation 12), which is obtained by averaging Equation 3 over the spiking noise (Figure 5B, red lines). The shape of this function indicates that connections are randomly created and deleted even when neurons are firing at their target rate. The larger the amplitude of the noise, the larger is the asymptotic variance of the process and the amount of spontaneous rewiring taking place.

We now extend our mean-field model of the rewiring process (see Section 2.3) to account for the spiking noise (see Section 4.5). According to the enhanced model, both the overshoot and the decay now match very well with numerical simulations of plastic networks (Figure 5C). The decay of connectivity following its overshoot is exponential (Figure 2.4D), and Equation 3 reveals that the homeostasis is multiplicative and that the decay rate should be constant. The exponential nature of the decay is best understood by inspecting the phase space (Figure 5F and G). In terms of connectivity, the learning process is qualitatively the same as in the noise-less case (Figure 4E), where a small perturbation leads to a fast relaxation to the line attractor (see Equation 16 in Section 4.7). In the presence of spiking noise (Figure 5F), however, the line attractor is deformed into a slow stochastic manifold (see Equation 18 in Section 4.8). The process of memory decay corresponds to a very slow movement toward the most entropic stable configuration compatible with firing rates clamped at their target value (Figure 5G). In our case, this leads to a constraint on the in-degree $K^{\text{in}} = \epsilon N_E$. We summarize the memory decay process by the equation

$$\begin{aligned} \mathbb{P}_L[C^*_{ij}] &\xrightarrow{\tau_{\text{diffusion}}} C^*_{ij} = \text{const.} \times K^{in}_i K^{out}_j = \frac{K^{in}}{N_E}, \\ \mathbb{P}_L[C^*_{ij}] &\xleftarrow{\tau_{\text{drift}}} C^*_{ij} + \text{Stimulus}. \end{aligned} \tag{5}$$

The fast "drift" process of relaxation back toward the slow manifold corresponds to the deterministic part of Equation 3. In contrast, the slow "diffusion" process of memory decay along the slow manifold corresponds to the stochastic part of Equation 3. In the equation above, τ_{drift} represents the time scale of the fast drift process, and $\tau_{\text{diffusion}}$ is the time scale of the slow diffusion process.

The drift process is strongly non-linear, and its bandwidth is limited by the time constant of the calcium filter τ_{Ca}, but also by the growth parameters of the dendritic elements β_d and axonal elements β_a. The diffusion process, on the other hand, is essentially constrained to the slow manifold of constant in-degree and firing rate (Section 4.8). Analytic calculations yield the relation

$$\tau_{\text{diffusion}} = \sqrt{\frac{4\pi\tau_{\text{Ca}}}{\eta^2\nu}} \frac{N_E c}{\frac{1}{\beta_d} + \frac{1}{\beta_a}} \tag{6}$$

where N_E is number of excitatory neurons, c is the average connectivity between excitatory neurons, and η is a correction factor to account for the reduced irregularity of spike trains as compared to a Poisson process. Both size and connectivity of the network increase the longevity of stored memories. Assuming that neurons rewire at a constant speed, it takes more time to rewire more elements. There is an interesting interference with the noise process, as memory longevity depends on the time constant of calcium in proportion to $\sqrt{\tau_{\text{Ca}}}$ (Figure 5 E). On the other hand, the time scale of learning τ_{drift} is limited by the low-pass characteristics of calcium, represented by τ_{Ca}. Increasing τ_{Ca}, which leads to more persistent memories, will eventually make the system unresponsive and prevent learning. We also find that the longevity of memories depends as $\frac{1}{\sqrt{\nu}}$ on the target rate. Therefore, making the target rate small enough should lead to very persistent memories. This path to very stable memories is not viable, though, because the average connectivity c implicitly changes with target rate. In Figure 5E longevity

of the memory is depicted as a function of the target rate with corrected connectivity $c = c(\nu)$, and we find that for very small target rates memory longevity tends to zero instead. This suggests that there is an optimal range of target rates centered at a few spikes per second, fully consistent with experimental recordings from cortical neurons [8].

To summarize, the process of forming an engram ("learning", see Section 2.3) exploits the properties of a line attractor. Taking spiking noise into account, the structure of the line attractor is deformed into a slow stochastic manifold. This still allows learning, but introduces controlled "forgetting" as a new feature. Forgetting is not necessarily an undesirable property of a memory system. In a dynamic environment, it might be an advantage for the organism to forget non-persistent or unimportant aspects of it. Homeostatic plasticity implements a mechanism of forgetting with an exponential time profile. Strong memories will be sustained longer, but they will eventually also be forgotten. In the framework of this model, the only way to keep memories forever is to repeat the corresponding stimulus from time to time, as illustrated in Figure 1D. If we think of the frequency of occurrence as a measure of the relevance of a stimulus, this implies that irrelevant memories decay and relevant ones remain. Memories are stored in a distributed fashion in the slow manifold of the system, instead of being stored in individual synaptic connections [33]. Forgetting is reflected by a diffusion to the most entropic network configuration along the slow manifold. As a result, the system performs continuous inference from a persistent stream of information about the environment. Already stored memories are constantly refreshed in terms of a movement in directions away from the most entropic point of the slow manifold (novel memories define new directions), while diffusion pushes the system back to the most entropic configuration.

2.5 Network stability and constraints on growth parameters

So far, we have described the process of forming and maintaining memory engrams based on homeostatic structural plasticity. We have explained the mechanisms behind the striking associative properties of the system. Now, we will explore the limits of stability of networks with homeostatic structural plasticity and derive meaningful parameter regimes for a robust memory system. A homeostatic controller that operates on the basis of firing rates can be expected to be very stable by construction. Indeed we find that, whenever parameters are assigned meaningful values, the Jacobian obtained by linearization of the system around the stable mean connectivity $\mathcal{J} = \mathcal{J}(\epsilon)$ has only eigenvalues λ with non-positive real parts $\mathrm{Re}[\lambda] \leq 0$ (see Section 4.9). As a demonstration, we consider the real part of the two "most unstable" eigenvalues as a function of two relevant parameters, the dendritic/axonal growth parameter β_d and the calcium time constant τ_{Ca} (Figure 6B, upper panel). The real part of these eigenvalues remains negative for any meaningful choice of time constants. It should be noted at this point, however, that the system under consideration is strongly non-linear, and linear stability alone does not guarantee global stability. We will discuss an interesting case of non-linear instability in Section 2.6. Oscillatory transients represent another potential issue in general control systems, and we will now explore the damped oscillatory phase of activity in more detail.

In Figure 6A we depict three typical cases of homeostatic growth responses: non-oscillatory (left, green), weakly oscillatory (middle, blue), and strongly oscillatory (right, red) network remodeling. The imaginary parts of the two eigenvalues shown in Figure 6B (bottom left), which are actually responsible for the oscillations, become non-zero when the dendritic and axonal growth parameters are too small (for other parameters, see Section 2.3), and both creation and deletion of elements are too fast. Oscillations occur, on the other hand, for large values of the calcium

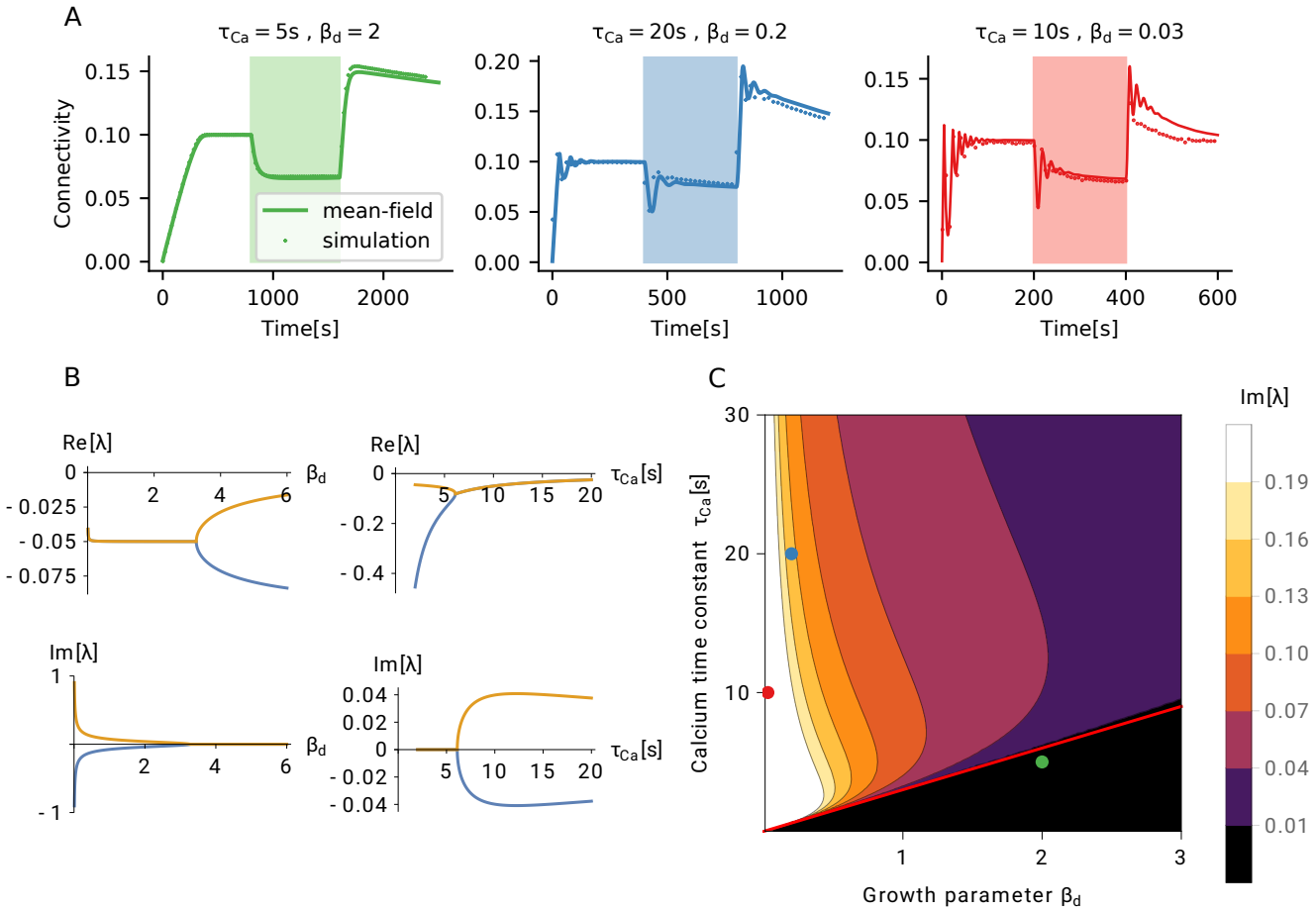

Figure 6: Linear stability of a network with homeostatic structural plasticity. (A) For a wide parameter regime, the structural evolution of the network has a single fixed point, which is also stable. Three typical types of homeostatic growth responses are depicted for this configuration: non-oscillatory (left), weakly oscillatory (middle), and strongly oscillatory (right) network remodeling. (B) All eigenvalues of the linearized system have a negative real part, for all values of the growth parameters of dendritic (axonal) elements β_d and calcium τ_{Ca}. In the case of fast synaptic elements (small β_d) or slow calcium (large τ_{Ca}), the system exhibits oscillatory responses. Shown are real parts and imaginary parts of the two "most unstable" eigenvalues, for different values of β_d (left column, $\tau_{\mathrm{Ca}} = 10\,\mathrm{s}$) and τ_{Ca} (right column, $\beta_d = 2$). (C) Phase diagram of the linear response. The black region below the red line indicates non-oscillatory responses, which corresponds to the configuration $\tau_{\mathrm{Ca}} \leq 3\beta_d\,\mathrm{s}$. Dots indicate the parameter configurations shown in panel (A), with matching colors.

time constant τ_{Ca} (Figure 6B, bottom right). The system oscillates, if the low-pass filter is too slow as compared to the turnover of synaptic elements. The combination of β_d and τ_{Ca} that leads to the onset of oscillations can be derived from the condition $\mathrm{Im}[\lambda] = 0$. We can further exploit the fact that two oscillatory eigenvalues are complex conjugates of each other, and that the imaginary part is zero, when the real part bifurcates.

To elucidate the relative importance of the two parameters β_d and τ_{Ca}, we now explore how they together contribute to the emergence of oscillations (Figure 6C). The effect of parameters on oscillations is a combination of the two mechanisms discussed above: low-pass filtering and agility of control. We use the bifurcation of the real part of the least stable eigenvalues as a criterion for the emergence of $\mathrm{Im}[\lambda] = 0$, which yields the boundary between the oscillatory and the non-oscillatory region (Figure 6C, red line). The black region of the phase diagram corresponds

to a simple fixed point with no oscillations, the green point corresponds to the case shown in Figure 6A, left. From Figure 6B, bottom, we conclude that the fastest oscillations are created when β_d is very small, as the oscillation frequency then exhibits a $\frac{1}{\beta_d}$ asymptotic dependence. The calcium dependence is a slowly changing function. The specific case indicated by a red point in Figure 6C corresponds to the dynamics shown in Figure 6A, right. Although intermediate parameter values result in damped oscillations (Figure 6C, blue dot; Figure 6A, middle), its amplitude remains relatively small. This link between two parameters can be used to predict a meaningful range of values for β_d. Experimentally reported values for τ_{Ca} are combined with the heuristic of not exhibiting strong oscillations.

The analysis outlined in the previous paragraph clearly suggests that, in order to avoid excessive oscillations, the calcium signal (a proxy for neuronal activity) has to be faster than the process which creates elements. Oscillations in network growth are completely suppressed, if it is at least tree times faster. Strong oscillations can compromise non-linear stability, as we will show in Section 2.6. This is a dynamic regime to be strictly avoided by the controller, for reasons explained later. We assume that the calcium time constant is in the range between 1 s and 10 s, in line with the values reported for somatic calcium transients in experiments [16, 17, 20, 49]. This indicates that homeostatic structural plasticity should not use element growth parameters smaller than around 0.4. Faster learning must be based on other types of synaptic plasticity (e.g. spike-timing dependent plasticity, or fast synaptic scaling).

We use this analysis framework now to compute turnover rates (TOR) and compare them to the values typically found in experiments. In Sections 2.3 and 2.4 we use a calcium time constant of 10 s and a growth parameters for synaptic elements of $\beta_a = \beta_d = 2$, which results in TOR of around 18 % per day (see Methods). Interestingly, [41] measured TOR in the barrel cortex of young mice and found TOR values of around 20 % per day. After sensory deprivation, the TOR increased to a maximum of around 30 % per day in the barrel cortex (but not elsewhere). In our model, stimulus-dependent rewiring is strongest in the directly stimulated engram E_1 (Figure 4C). This particular ensemble rewires close to 25 % of its dendritic elements per stimulation cycle.

2.6 Loss of control leads to bursts of high activity

A network the connectivity of which is subject to homeostatic regulation generally exhibits robust linear stability around the fixed point of connectivity ϵ, as explained in detail in Section 2.5 and Section 4.9. But what happens, if the system is forced far away from its equilibrium? To illustrate the new phenomena arising, we repeat the stimulation protocol described in Section 2.3 with one stimulated ensemble E_1. However, we now increase both the strength and the duration of the stimulation (Figure 7A). The network behaves as before during the growth and the stimulation phase (Figure 7A, upper panel), but during the reconsolidation phase connectivity gets out of control. New recurrent synapses are formed at a very high rate until excessive feedback of activity triggered by input from the non-stimulated ensemble causes an explosion of firing rates (Figure 7A bottom panel). The homeostatic response of the network to such seizure-like activity can only be a brisk decrease in recurrent connectivity. As a consequence, the activity r_{E_1} quickly drops to zero and the deregulated growth cycle starts all over.

We explore the mechanism underlying this runaway process by plotting the long-term dynamics in a phase plane spanned by recurrent connectivity $C_{E_1E_1}$ and the activity of the engram r_{E_1} (Figure 7B). A special type of limit cycle emerges, and we can track it using the input connectivity from the rest of the network to the learned engram

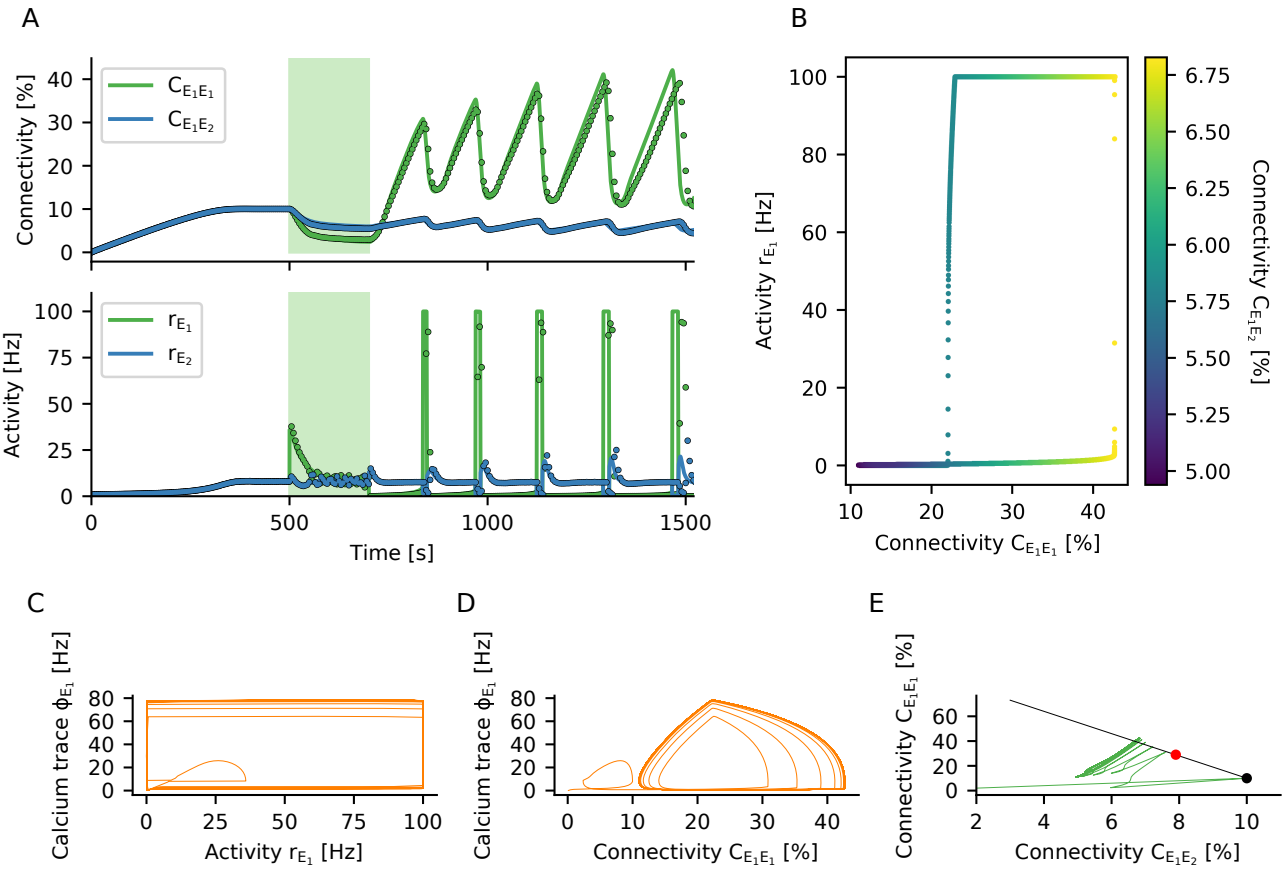

Figure 7: Non-linear stability of a network with homeostatic structural plasticity. (A) The engram E_1 is stimulated with a very strong external input. As the homeostatic response triggers excessive pruning of recurrent connections, the population E_1 is completely silenced after the stimulus is turned off. This, in turn, initiates a strong compensatory overshoot of connectivity and consecutive runaway population activity. The dots with corresponding color show the results of a plastic network simulation, and the solid lines indicate the corresponding predictions from our theory. The theoretical instantaneous firing rate is clipped at 100 Hz. (B) The network settles in a limit cycle of connectivity dynamics. The hysteresis-like behavior is caused by the faster growth of within-engram connectivity $C_{E_1E_1}$ as compared to connectivity from the non-engram ensemble $C_{E_1E_2}$. During the initial phase of the cycle, the increase of $C_{E_1E_1}$ has no effect on the activity of population E_1 yet, as its neurons are not active. Only when the input from population E_2 through $C_{E_1E_2}$ gets large enough, the rate r_{E_1} becomes non-zero and rises to very high values quickly due to already large recurrent $C_{E_1E_1}$ connectivity. (C) The calcium signal ϕ adds an additional delay to the cycle. (D) This leads to smoother trajectories when scattering calcium concentration against connectivity. (E) Connectivity within the stimulated group $C_{E_1E_1}$ plotted against input connectivity from the non-engram population $C_{E_1E_2}$. The black line shows configurations with constant in-degree, of which the black dot represents the most entropic one. The red dot corresponds to critical connectivity, beyond which the limit cycle behavior is triggered. The limit cycle transients in connectivity space are orthogonal to the line attractor, indicating that the total in-degree is oscillating and no homeostatic equilibrium can be established.

($C_{E_1E_2}$, see Figure 7B). The cycle is started when the engram E_1 is stimulated with a very strong external input. As the homeostatic response of the network triggers excessive pruning of its recurrent connections, the population E_1 is completely silenced, $r_{E_1} = 0$, after the stimulus has been turned off. Then, homeostatic plasticity sets in and tries to compensate the activity below target by increasing the recurrent excitatory input to the engram E_1. The growth of intra-ensemble connectivity $C_{E_1E_1}$ is faster than the changes in inter-ensemble connectivity $C_{E_1E_2}$, as the growth rate of $C_{E_1E_1}$ is quadratic in the rate r_{E_1} (Figure 4G), but $C_{E_1E_2}$ depends only linearly on it. However, while there are no recurrent spikes, $r_{E_1} = 0$, the increase in intra-ensemble connectivity cannot restore the activity to its target value. As soon as input from the rest of the network via $C_{E_1E_2}$ is strong enough to increase the rate r_{E_1} to non-zero values, engram neurons very quickly increase their own rate by activating recurrent connectivity $C_{E_1E_1}$. At this point, however, the network has entered a second attractor of connectivity, coinciding with a pronounced outbreak of population activity r_{E_1}. The increase in rate is then immediately counteracted by the homeostatic controller. Due to the seizure-like activity burst, a high amount of calcium is accumulated in all participating cells. As a consequence, neurons delete many excitatory connections, and the firing rates are driven back to zero. This hysteresis-like cycle of events is repeated over and over again (Figure 7B), even if the stimulus has meanwhile been turned off. The period of the limit cycle is strongly influenced by the calcium variable, which lags behind activity (Figure 7C). Replacing activity r_{E_1} by recurrent connectivity $C_{E_1E_1}$, a somewhat smoother picture emerges (Figure 7D).

Two aspects are important for the emergence of the limit cycle. Firstly, the specific relation between the time scales of calcium and synaptic elements gives rise to different types of instabilities (see Figure 6 and Figure 7C and D). Secondly, the rates of creation and deletion of elements do not have the same bounds. While the rate with which elements are created ρ^+ is limited by $\frac{1}{\beta_d}\nu$, the rate of deletion ρ^- is limited by $\frac{1}{\beta_d}\frac{1}{\tau_{\text{ref}}}$. This peculiar asymmetry causes the observed brisk decrease in connectivity after an extreme seizure-like burst of activity. An appropriate choice of the calcium time constant, in combination with a strict limit on the rate of deletion, might lead to a system without the (pathological) limit cycle behavior observed in simulations. Finally, we have derived a criterion for bursts of population activity to arise, related to the loss of stability due to excessive recurrent connectivity (see Section 4.9, Equation 22). Indeed, a network with fixed in-degrees becomes dynamically unstable, if its connectivity $C_{E_1E_1}$ exceeds the critical value $C^{\text{crit}}_{E_1E_1} = \epsilon(1 + \frac{N_{E2}}{N_{E1}j_E})$, which for our parameters is at about 29 %. The neurons comprising the engram E_1 receive too much recurrent input (Figure 7E), and the balance of excitation and inhibition brakes. In this configuration, only one attractive fixed point exists for high firing rates, and a population burst is inevitable. In simulations, the stochastic nature of the system tends to elicit population bursts even earlier, at about 22 % connectivity in our hands. We conclude that 22–29 % connectivity is a region of bi-stability, with two attractive fixed points coexisting. Early during limit cycle development, the total in-degree is less than ϵN (the connectivity is in the region below the black line in Figure 7E), and the excitation-inhibition balance is broken by positive feedback. Later, the limit cycle settles into a configuration, where the total in-degree exceeds ϵN (the black line is crossed from below in Figure 4E). We have shown before that stable learning leads to silent memories in the network (Section 2.1 and 2.2), but in the case discussed here, sustained high activity is at odds with stable homeostatic control of network growth.

3 Discussion

We have demonstrated by numerical simulations and by mathematical analysis that structural plasticity controlled by firing rate homeostasis has the potential to implement a memory system based on the emergence and the decay of engrams. Input patterns are defined by stimulation of the corresponding ensemble of neurons in a recurrent network. Presenting two patterns concurrently leads to their association by newly formed synaptic connections. This mechanism can be used, among other things, to effectively implement classical conditioning. The memories are dynamic. They decay if previously learned stimuli are no longer presented, but they get stronger with every single recall. The memory is not affecting the firing rates during spontaneous activity, but even weak memory traces can be identified by the correlation of activity. Memories become visible as a firing rate increase of a specific pattern upon external stimulation, though. The embedding network is able to perform pattern completion, if a partial cue is presented. Finally, we have devised a simple recognition memory mechanism, in which downstream neurons respond with a higher firing rate, if any of the previously learned patterns is stimulated.

Memory engrams emerge, because the homeostatic rule acts as an effective Hebbian rule with associative properties. This unexpected behavior is achieved by an interaction between the temporal dynamics of homeostatic control and a network-wide distributed formation of synapses. Memory formation is a fast process, exploiting degrees of freedom orthogonal to a line attractor as it reacts to the stimulus, and storing memories as positions on the line attractor. The spiking of neurons introduces fluctuations, which lead to the decay of memory on a slow time scale through diffusion along the line attractor. In absence of specific stimulation, the network relaxes to the most entropic configuration of uniform connectivity across all pairs of neurons. In contrast, multiple repetitions of a stimulus pushes the system to states of lower entropy, corresponding to stronger memories. The dynamics of homeostatic networks is, by construction, very robust for a wide parameter range. Instabilities occur when the time scales of creating and deleting synaptic elements are much smaller than the time scales of the calcium trace, which feeds the homeostatic controller. Under these conditions, the network displays damped oscillations, but remains linearly stable. Stability is lost, though, when the stimulus is too strong. In this case, the compensatory forces lead to limit cycle dynamics with pathologically large amplitudes.

Experiments involving engram manipulation have increased our current knowledge about this type of memory [24], and some of these findings are actually in accordance with our model. For example, memory re-consolidation was disrupted if a protein synthesis inhibitor was administered immediately after the retrieval cue during an auditory fear conditioning experiment [34]. In our model, engram connectivity initially decreases upon stimulation, and memories are shortly destabilized and consolidated again after every retrieval. Interfering with plasticity during or after retrieval can, therefore, also lead to active forgetting. It was also shown in experiments that neurons are more likely to be allocated to an engram, if they are more excitable before stimulation [45, 48]. In our model, more excitable neurons would fire more during stimulation, making them more likely to become part of an engram. Moreover, our analysis of the model suggests that decreasing excitability of some neurons soon after stimulation should also increase the likelihood of them becoming part of the engram. Further research with our model of homeostatic engram formation might include even more specific predictions for comparison with experiments involving engram manipulation. This would also help to better characterize and understand the process of engram formation in the brain.

High turnover rates of synapses increases the volatility of network structure. This, in turn, poses a grand challenge

to any synaptic theory of memory [33], and it is not yet clear how memories can at all persist in a system that is constantly rewiring. In our model, the desired relative stability of memories is achieved by storing them with the help of a slow manifold mechanism. An estimation of turnover rates in our model amounts to about 18 % per day, which is comparable to the 20 % per day that have been measured in mouse barrel cortex [41]. In general, however, adult mice have more persistent synapses with much lower turnover rates as low as 4 % per month [31, 50, 21]. This can be accounted for in our model, as increased growth parameters of axonal, β_a, and dendritic, β_d, elements would lead to smaller synaptic turnover rates and, consequently, to more persistent spines (see Methods). The downside of increasing the growth parameters is that the learning process becomes slower. The turnover rate of 18 % per day corresponds to a specific value of the parameter β_d. It is conceivable, however, to implement an age-dependent parameter β_d. For example, one could have a high turnover rate in the beginning and let the growth become slower with time. This would reflect the idea that the brains of younger animals are more plastic than the brains of older ones. As animals grow older, synapses become more persistent. Similar to certain machine learning strategies ("simulated annealing"), this could be the optimal strategy for an animal, which first explores a given environment and then exploits the acquired adaptations to thrive in it.

Recently, [10] showed that Hebbian structural plasticity could be the force behind memory consolidation through a process of stabilization of connectivity, which is based on the existence of an attractive fixed point in the plastic network structure. In our model, because of the decay of the slow manifold, memories are never permanent, and repeated stimulation is necessary to stabilize them. We would argue, though, that forgetting is an important aspect of any biological system. In our case, we observe an exponential decay, if the stimulus is no longer presented. Furthermore, using a similar structural plasticity model, it was shown that a network can repair itself after lesion [2]. Together with our results, this suggests that a structural perturbation of engrams (e.g. by removing connections or deleting neurons) could actually trigger "healing" and a rescue of memories. In the case of unspecific lesions, however, such perturbation might also lead to the formation of "fake" memories, or to the false association of actually unconnected memories.

It appears that the attractor metaphor of persistent activity is not consistent with our model of homeostatic plasticity. As explained in Section 2.6, homeostatic control tends to delete connections between neurons which are persistently active, and in extreme cases could even lead to pathological oscillations. In the case discussed in Section 2.2, in contrast, the memories formed are "silent" (elsewhere classified as "transient" [38]), very different from the persistent activity usually considered in working memory tasks (elsewhere classified as "persistent", or "dynamic" [38]). The latter type of activity seems to be consistent with Hebbian plasticity models [10, 30, 46], and one may wonder what is the relation of our model with these alternative models.

One possible way to integrate both mechanisms in a single network would be to keep their characteristic time scales separate. This could be accomplished, for example, by choosing faster time constants for Hebbian functional plasticity, and slower ones for homeostatic structural plasticity. An effective separation of time scales could also be obtained, if homeostatic structural plasticity would use somatic calcium as a signal, but not exert any control of the intermediate calcium levels [18]. This would eliminate the need to specify a target rate in the model, and fast functional plasticity would shape connectivity in the allowed range of values where neurons have a distribution of firing rates reflecting previous experience. This induces a natural separation of time scales, where memories encoded by homeostatic plasticity would last much longer than in the present model, as only extreme transients would trigger rewiring. Homeostatic plasticity would perform Bayesian-like inference similar to structure learning,

while functional plasticity would perform fast associative learning, similar to the system proposed by [13].

We showed that very strong stimulation can damage the network by deleting too many synapses in a short time. The compensatory force, which normally guarantees stability, becomes too strong and leads to seizure-like bursts of very high activity. This pathological behaviour of the overstimulated system could be relevant for the study of certain brain diseases, such as epilepsy. The disruption of healthy stable activity is caused by a broken excitation-inhibition balance due to the high activity of one subgroup (Figure 7A). This, in turn, leads to the emergence of an abnormal connectivity cycle (Figure 7E). Strategies for intervention in this case must take the whole cycle into account, and not just the phase of extreme activity. Inhibiting neurons during the high-activity phase, for example, could have an immediate effect, but it would not provide a sustainable solution to the problem of runaway connectivity. Our results suggest, against intuition maybe, that additional excitation of the highly active neurons could actually terminate the vicious cycle quite efficiently. It is important to note, however, that our system has not been designed as a model of epilepsy, and therefore does not reproduce all features of it [36]. In particular, seizure occurrence is stochastic in nature, but the limit cycle we describe here implies periodic activity. Furthermore, the process in real tissue is accompanied by other structural changes such as neuronal death and glia-related reorganization. In any case, our results do shed light on a novel mechanism of pathological overcompensation and could potentially instruct alternative approaches in future epilepsy research.

René Descartes already proposed a theory of memory, paraphrased in [33]: Putting needles through a linen cloth would leave traces in the cloth that either stay open, or can more easily be opened again. Richard Semon, who originally coined the term "engram" in his book [24, 37], proposes that an engram is a "permanent record" formed after a stimulus impacts an "irritable substance". Putting these two ideas together, we can think of Descartes' needles not to penetrate an inanimate linen cloth, but a living brain, the irritable substance. In this case, we should expect the formation not of permanent holes, but of scar tissue, which grows further by repeating the procedure. Therefore, the memory of the system is just a "scar" left by sensory experience. We think that this is a good metaphor for the type of memories described in our paper, formed through homeostatically controlled structural plasticity. Interestingly, this model was originally meant as a model for rewiring after lesion [2]. In our work, however, the "lesion" is imposed by stimulation, which induces phenomena similar to scar formation. The dynamics of this healing process is very universal, where resources from the whole network are used to fix a local problem leading to a scar. A perturbation introduces heterogeneity in a previously homogeneous organic substrate.

4 Methods

4.1 Network model

The neuronal network consists of $N_E = 10\,000$ excitatory and $N_I = 2\,500$ inhibitory current-based leaky integrate-and-fire (LIF) neurons. The sub-threshold dynamics of the membrane potential V_i of neuron i obeys the differential equation

$$\tau_m \frac{dV_i}{dt} = -V_i + \tau_m \sum_j C_{ij} J_{ij} S_j(t - D). \tag{7}$$

The membrane time constant τ_m is the same for all neurons. The number of synaptic contacts between a presynaptic neuron j and a postsynaptic neuron i is denoted by C_{ij}. The synaptic weights of individual contacts J_{ij} is the peak amplitude of the postsynaptic potential and depends only on the type of the presynaptic neuron. Excitatory

connections have a strength of $J_E = J = 0.1\,\mathrm{mV}$. Inhibitory connections are stronger by a factor $g = 8$ such that $J_I = -gJ = -0.8\,\mathrm{mV}$. A spike train $S_j(t) = \sum_k \delta(t - t_j^k)$ consists of all spikes produced by neuron j. The external input to a given neuron in the network is conceived as a Poisson process of rate $\nu_{\mathrm{ext}} = 15\,\mathrm{kHz}$. The external input to different neurons is assumed to be independent. All synapses have a constant transmission delay of $D = 1.5\,\mathrm{ms}$. When the membrane potential reaches the firing threshold $V_{\mathrm{th}} = 20\,\mathrm{mV}$, the neuron emits a spike that is transmitted to all postsynaptic neurons. Its membrane potential is then reset to $V_r = 10\,\mathrm{mV}$ and held there for a refractory period of $t_{\mathrm{ref}} = 2\,\mathrm{ms}$.

The number of input synapses is fixed at $0.1N_I$ for inhibitory-to-inhibitory and inhibitory-to-excitatory connections, and at $0.1N_E$ for excitatory-to-inhibitory synapses. Once synaptic connections of these three types are established, they remain unchanged throughout the simulation. In contrast, excitatory-to-excitatory connections are initially absent and grow only under the control of a structural plasticity rule.

4.2 Plasticity model

Growth and decay of excitatory-to-excitatory (EE) connections follow a known model of structural plasticity regulated by firing rate homeostasis [2, 12]. In this model, each neuron i has a certain number of synaptic elements of two kinds available, axonal elements $a_i(t)$ and dendritic elements $d_i(t)$. These elements are bonded together to create functional synapses. Synaptic elements that have not yet found a counterpart are called free elements, denoted by a_i^+ and d_j^+, respectively. If $K_i^{\mathrm{in}} = \sum_j C_{ij}(t)$ denotes the in-degree and $K_i^{\mathrm{out}} = \sum_j C_{ji}(t)$ the out-degree of neuron i, the number of free elements in every moment is given by $a_i^+(t) = [a_i(t) - K_i^{\mathrm{out}}(t)]_+$ and $d_i^+(t) = \left[d_i(t) - K_i^{\mathrm{in}}(t)\right]_+$, with $[x]_+ = \max(x, 0)$.

Firing rate homeostasis is implemented by allowing each neuron to individually control the number of its synaptic elements. We assume that each neuron i maintains a time-dependent estimate of its own firing rate, using its intracellular calcium concentration $\phi_i(t)$ as a proxy. This variable reflects the spikes $S_i(t)$ the neuron has generated in the past, according to

$$\tau_{\mathrm{Ca}}\dot{\phi}_i(t) = -\phi_i(t) + S_i(t),$$

with a time constant of $\tau_{\mathrm{Ca}} = 10\,\mathrm{s}$ for all neurons. This implements a first-order low-pass filter. In this model, more weight is given to more recent spikes, following a decaying exponential. The calcium trace $\phi_i(t)$ of individual neurons is used as a control signal for the number of axonal elements $a_i(t)$ and dendritic elements $d_i(t)$ according to the homeostatic equations

$$\beta_d\dot{b}_i(t) = \nu_i - \phi_i(t) \qquad \beta_a\dot{a}_i(t) = \nu_i - \phi_i(t),$$

where β_d is the dendritic and β_a is the axonal growth parameter. Both have a value of 2 in our default setup. The parameter ν_i is called the target rate. Whenever the firing rate estimate (in fact, the calcium concentration) is below the target rate, the neuron creates new axonal and dendritic elements, from which new synapses can be formed. Whenever the estimated firing rate is larger than the target rate, the neuron deletes some of its elements, removing the synapses they form. The (negative) decrements a_i^- and d_i^- in the number of synaptic elements, respectively, are in each moment given by $a_i^-(t) = [a_i(t) - K_i^{\mathrm{out}}(t)]_-$ and $d_i^-(t) = \left[d_i(t) - K_i^{\mathrm{in}}(t)\right]_-$ for $[x]_- = \min(x, 0)$.

After time intervals of duration ΔT_s, all negative elements are collected, and a_i^- of the existing outgoing connections of neuron i are randomly deleted. Similarly d_i^- connections are randomly deleted. The deletion of bonded elements

of one type frees their counterparts that were previously connected to the deleted element. Then, all free dendritic $|\mathbf{d}^+|$ and axonal elements $|\mathbf{a}^+|$ are collected and randomly combined into pairs, creating $n = \min(|\mathbf{a}^+|, |\mathbf{d}^+|)$ new synaptic connections. This algorithm has originally been devised by [2], an efficient implementation of it in NEST exists [9] and has been employed for all our simulations.

4.3 Mathematical re-formulation of the algorithm

The algorithm of homeostatically controlled structural plasticity can be expressed as a discrete-time stochastic process. Rewiring takes place at regular intervals of duration ΔT_s

$$T_{\text{rewire}} = \{t_0 = 0, t_1 = \Delta T_s, t_2 = 2\Delta T_s, \dots, t_n = n_T \Delta T_s\}.$$

Between any two rewiring events, for $t \in (t_k, t_k + \Delta T_s)$, the neuron just accumulates synaptic elements

$$\begin{aligned} \Delta C_{ij}(t) &= 0 \\ a_i(t) &= \int_{t_k}^{t} \frac{1}{\beta_a}(\nu_i - \phi(t'))\, dt' \\ d_i(t) &= \int_{t_k}^{t} \frac{1}{\beta_d}(\nu_i - \phi_i(t'))\, dt' \end{aligned}$$

while the already established connectivity remains unchanged. At every rewiring step, the rearrangement of connectivity is completely random, driven by the probabilities $P(\Delta_\pm C_{ij}(t_k) = c|\mathbf{a}(t_k), \mathbf{d}(t_k), \mathbf{C}(t_{k-1}))$ of creating or deleting c connections from neuron j to neuron i at time t_k, during a time step of duration ΔT_s. This gives rise to a discrete-time Markov process

$$C_{ij}(t_k) = C_{ij}(t_{k-1}) + \Delta_+ C_{ij}(t_k) - \Delta_{a^-} C_{ij}(t_k) - \Delta_{d^-} C_{ij}(t_k),$$

for $t_k \in T_{\text{rewire}}$. Here, we define $\Delta_+ C_{ij}(t_k)$ as the random variable representing the creation of synapses, while $\Delta_{a^-} C_{ij}(t)$ and $\Delta_{d^-} C_{ij}(t)$ are random variables describing the deletion of synapses by removing their corresponding axonal and dendritic elements, respectively.

We first calculate the probability to create just one new connection $p_{ij}^+(t_k) = P(\Delta_+ C_{ij}(t_k) = 1|\mathbf{a}(t_k), \mathbf{d}(t_k), \mathbf{C}(t_{k-1}))$. We can express this as a process of selecting a presynaptic partner j with probability $P(\text{presynaptic neuron} = j) = \frac{a_j^+(t_k)}{|\mathbf{a}^+(t_k)|}$ and then a postsynaptic partner i with probability $P(\text{postsynaptic neuron} = i) = \frac{d_i^+(t_k)}{|\mathbf{d}^+(t_k)|}$. We then connect the pair with the product of both probabilities

$$p_{ij}^+(t_k) = \underbrace{\frac{d_i^+(t_k)}{|\mathbf{d}^+(t_k)|}}_{\text{prob. of choosing a post neuron}} \times \underbrace{\frac{a_j^+(t_k)}{|\mathbf{a}^+(t_k)|}}_{\text{prob. of choosing a pre neuron}}$$

as they are independent random variables. We now have the probability of creating individual connections, but the full probability of an increment for the whole network is hard to calculate. This is because of statistical dependencies that arise from the fact that rewiring affects all neurons in the network simultaneously. First, the total number of new connections is $n = \min(|\mathbf{a}^+|, |\mathbf{d}^+|)$. Second, the number of new connections for a given pair of neurons is bounded by the number of free axonal and dendritic elements in the two neurons, respectively, $n_{ij} = \min(d_i^+, a_j^+)$. Finally, we cannot delete more connections than we actually have. This indicates that independent combinations of individual probabilities cannot be expressed by simple binomial distributions, but a hypergeometric distribution arises instead. We obtain for the probability of creating c synapses from neuron j to neuron i

$$P(\Delta_+ C_{ij}(t_k) = c|\mathbf{a}(t_k), \mathbf{d}(t_k), \mathbf{C}(t_{k-1})) = \frac{\binom{d_i^+(t_k) a_j^+(t_k)}{c} \binom{|\mathbf{a}^+(t_k)||\mathbf{d}^+(t_k)| - d_i^+(t_k) a_j^+(t_k)}{n(t_k) - c}}{\binom{|\mathbf{a}^+(t_k)||\mathbf{d}^+(t_k)|}{n(t_k)}}.$$

This probability is easy to understand: We divide the ensemble of all possible new synapses (which has size $|\mathbf{a}^+||\mathbf{d}^+|$) into the ensemble of potential synapses between the pair (i,j) (which has size $d_i^+ a_j^+$) and all the rest. We then choose $c_{ij} < n_{ij}(t_k)$ connections from the preferred ensemble, and the rest of connections from the remaining pool. This is "sampling without replacement" as there is a fixed number of new connections $n(t_k)$ in each time step.

We can now calculate the probability to delete one connection using axonal "negative" elements as $p_{ij}^{a^-}(t_k) = P(\Delta_{a^-} C_{ij}(t_k) = 1|\mathbf{a}(t_k), \mathbf{C}(t_{k-1}))$. This is the probability to choose one to-be-deleted element from all existing elements $p_{ij}^{-a}(t_k) = \frac{a_i^-(t_k)}{a_i(t_k)}$ and $p_{ij}^{d^-}(t_k) = P(\Delta_{d^-} C_{ij}(t_k) = 1|\mathbf{d}(t_k), \mathbf{C}(t_{k-1})) = \frac{d_i^-(t_k)}{d_i(t_k)}$. Out of $a_i(t_k)$ candidates for deletion, we select $a_i^-(t_k)$, subject to the condition not to delete more than $C_{ij}(t_k)$ for this particular pair of neurons. This constraint is reflected by the hypergeometric distribution. The preferred population is represented by the elements bonded into connections from neurons j to neuron i, and the other population is comprised by all remaining elements of neuron j. Finally, during rewiring events in T_{rewire}, we obtain for the stochastic evolution of $C_{ij}(t_k)$

$$\begin{aligned}
C_{ij}(t_k) &= C_{ij}(t_{k-1}) + \Delta_+ C_{ij}(t_k) - \Delta_-^a C_{ij}(t_k) - \Delta_-^b C_{ij}(t_k) \\
\Delta_+ C_{ij}(t_k) &\sim \text{Hypergeometric}\left(\Delta_+ C_{ij}(t_k) = c | d_i^+(t_k) a_j^+(t_k), |\mathbf{d}^+||\mathbf{a}^+|, \min(|\mathbf{a}^+|, |\mathbf{d}^+|)\right) \\
\Delta_-^a C_{ij}(t_k) &\sim \text{Hypergeometric}\left(\Delta_+ C_{ij}(t_k) = c | a_j^-(t_k), a_j(t_k), C_{ij}(t_{k-1})\right) \\
\Delta_-^b C_{ij}(t_k) &\sim \text{Hypergeometric}\left(\Delta_+ C_{ij}(t_k) = c | d_i^-(t_k), d_i(t_k), C_{ij}(t_{k-1})\right).
\end{aligned} \tag{8}$$

To calculate the total change $\Delta C_{ij}(t_k)$ we have to account for all these contributions. The distribution of the total increment is not simply the convolution of the three distributions given above, as they are not independent. On the contrary, (negative) decrements occasionally influence (positive) increments, as we first delete connections and thereby create additional free elements. Therefore, the number of free elements has to be corrected as

$$a'^+_i(t_k) = a_i^+(t_k) + \sum_l \Delta_-^b C_{li}(t_k), \qquad b'^+_i(t_k) = d_i^+(t_k) + \sum_l \Delta_-^a C_{il}(t_k).$$

Equation 8 defines a complicated discrete-time stochastic process, but since we are at this point interested only in the expected change of connectivity, we can restrict ourselves to the evolution of expectations. We use $\mathbb{E}_s$ to denote the (linear) operator of expectation over the structural noise, i.e. over the realizations of the increments/decrements $\Delta C_{ij}(t_k)$. We have

$$\mathbb{E}_s[\Delta C_{ij}(t_k)] = \frac{b'^+_i(t_k) a'^+_j(t_k)}{\max(|\mathbf{a}'^+(t_k)|, |\mathbf{b}'^+(t_k)|)} + \mathbb{E}_s[C_{ij}(t_{k-1})] \left(\frac{d_i^-(t_k)}{d_i(t_k)} + \frac{a_j^-(t_k)}{a_j(t_k)} \right). \tag{9}$$

Further on in this paper, for notational convenience, we write $C_{ij}(t_k)$ for the expectation $\mathbb{E}_s[C_{ij}(t_k)]$.

4.4 Time-continuous limit

We now switch over to continuous equations, which result from the limit $\Delta T_s \to 0$. In this case, we can express free elements and negative elements as

$$a_i^\pm(t) = \left[\frac{1}{\beta_a} (\nu_i - \phi_i(t)) dt \right]_\pm, \qquad d_i^\pm(t) = \left[\frac{1}{\beta_d} (\nu_i - \phi_i(t)) dt \right]_\pm,$$

which will assign infinitesimally small values to the numbers of free elements and negative elements. Since the rewiring takes place continuously, the numbers of elements are, up to infinitesimal correction, the same as the

degrees, $a_i \approx K_i^{\text{in}}$ and $d_i \approx K_i^{\text{out}}$. We can now define the rates of creation and deletion of axonal elements as $\rho_{a_i}^{\pm} = \lim_{dt\to 0} \frac{a_i^{\pm}}{dt}$ and dendritic of elements as $\rho_{d_i}^{\pm} = \lim_{dt\to 0} \frac{d_i^{\pm}}{dt}$ and we write explicitly

$$\rho_{a_i}^{\pm}(t) = \frac{1}{\beta_a}\left[\nu_i - \phi_i(t)\right]_{\pm}, \qquad \rho_{d_i}^{\pm}(t) = \frac{1}{\beta_d}\left[\nu_i - \phi_i(t)\right]_{\pm}. \tag{10}$$

As noted above, we have omitted here the expectation over the structural noise $\mathbb{E}_s$ from the notation. We can now calculate the evolution of connectivity from Equation 9 as

$$\dot{C}_{ij}(t) = \frac{\rho'^{+}_{d_i}(t)\rho'^{+}_{a_j}(t)}{\rho(t)} - C_{ij}(t)\left(\frac{\rho^{-}_{d_i}(t)}{K_i^{in}(t)} + \frac{\rho^{-}_{a_j}(t)}{K_j^{out}(t)}\right), \tag{11}$$

where $\rho(t) = \max(|\boldsymbol{\rho}'^{+}_{a}(t)|, |\boldsymbol{\rho}'^{+}_{d}(t)|)$. The specific implementation requires that the deletion of elements takes place first, with the corresponding synaptic partner remaining available as a free element to form new connections. After an axonal element has been deleted, the previously bonded dendritic element becomes a free element. This requires a correction on the rate of free elements

$$\rho'^{+}_{a_i}(t) = \frac{1}{\beta_a}\left[\nu_i - \phi_i(t)\right]_{+} + \sum_k \frac{\rho^{-}_{d_k}(t)}{K_k^{in}(t)} C_{ki}(t)$$
$$\rho'^{+}_{d_i}(t) = \frac{1}{\beta_d}\left[\nu_i - \phi_i(t)\right]_{+} + \sum_k C_{ik}(t) \frac{\rho^{-}_{a_k}(t)}{K_k^{out}(t)}.$$

4.5 Spiking noise

We assume that spike trains $S_i(t) = \sum_k \delta(t - t_k^i)$ reflect an asynchronous-irregular state of the network, so they can be modeled as a stochastic point process. As described in [1, 42], the coefficient of variation of the spike trains generated by a leaky integrate-and-fire neuron driven by Gaussian white noise current is given by

$$\mathrm{CV}(\mu, \sigma) = 2\pi(\nu_0\tau_m)^2 \int_{\frac{V_r-\mu}{\sigma}}^{\frac{V_\theta-\mu}{\sigma}} e^{x^2}\, dx \int_{-\infty}^{x} e^{y^2}(1 + \mathrm{erf}(y))^2\, dy,$$

where μ and σ are the parameters of the current input, and τ_m, V_r and θ are the parameters of the neuron, respectively. The configuration used here yields CV ≈ 0.7. A good approximation for spike trains of a given rate r and irregularity CV is obtained with a specific class of renewal processes, so-called Gamma processes. These have an ISI distribution $f(t) = H(t)\frac{\rho}{\Gamma(\alpha)}(\rho t)^{\alpha-1}e^{-\rho t}$, with parameters $\alpha = \frac{1}{\mathrm{CV}^2}$ and $\rho = \frac{r}{\mathrm{CV}^2}$.

In our model, the fluctuating intracellular calcium concentration is a shotnoise, a continuous signal that arises from a point process through filtering. Here, the point process has a mean rate ν, and the calcium signal is a convolution with an exponential kernel $F(t) = \Theta(t)\frac{1}{\tau_{\mathrm{Ca}}}e^{-\frac{t}{\tau_{\mathrm{Ca}}}}$. Campbell's theorem allows us compute the mean $\mu_{\mathrm{Ca}} = \frac{\mathbb{E}[N_T]}{T}\int_0^t F(s)\, ds = \nu$ and the variance $\sigma^2_{\mathrm{Ca}} = \frac{\mathrm{Var}[N_T]}{T}\int_0^t F(s)^2\, ds \approx \mathrm{CV}^2\frac{\nu}{2\tau_{\mathrm{Ca}}}$ of the calcium variable. Here we used the fact that spike count of Gamma process $N_T = \int_0^T S(t)\, dt$ has a mean $\mathbb{E}[N_T] = \nu T$ and a variance $\mathrm{Var}[N_T] \approx \frac{\sigma^2_{\mathrm{ISI}}}{\mu^3_{\mathrm{ISI}}}T = \frac{\nu}{\alpha}$, provided the observation time T is long enough [35]. As a consequence of the Central Limit Theorem, the amplitude distribution of the calcium signal is approximately Gaussian $\mathcal{N}(\mu_{\mathrm{Ca}}, \sigma^2_{\mathrm{Ca}})$, provided the mean spike rate is much larger than the inverse time constant of the calcium signal $\langle r_i(t)\rangle \gg \frac{1}{\tau_{\mathrm{Ca}}}$. In other words, if the mean firing rate is 8 Hz and the calcium constant is $\tau_{\mathrm{Ca}} = 10$ s, there are on average 80 spikes in the characteristic time interval τ_{Ca}.

We are actually interested in the equilibrium rates of free and negative elements in Equation 10. These rates are rectified versions of the shifted calcium trace, and in order to calculate them we resort to the ergodic theorem and to an adiabatic approximation. The former is a self-averaging property, according to which the time-averaged variable

for a long observation is equal to the equilibrium mean value $\frac{\int_0^T x_i(t)\,dt}{T} = \langle x_i \rangle_t$. The adiabatic property comes from the fact that spiking dynamics of a network is much faster than network remodeling due to structural plasticity. At every point in time, plasticity is driven by the average adiabatic rate. This implies that, at every point in time t, the structural plasticity sees the equilibrium distribution of the calcium trace $P_{\text{eq}}(\phi_i(t)) = \mathcal{N}(\mu_{\text{Ca}}(t), \sigma^2_{\text{Ca}}(t))$. The right-hand side of Equation 10 becomes

$$\begin{aligned}\langle \rho_{a_i}^{\pm}(t) \rangle &= \frac{1}{\beta_a} \langle [\nu_i - \phi_i(t)]_{\pm} \rangle = R^{\pm}_{\sigma_a}\left(\frac{\nu_i - \langle r_i(t) \rangle}{\beta_a}\right) \\ \langle \rho_{d_i}^{\pm}(t) \rangle &= \frac{1}{\beta_d} \langle [\nu_i - \phi_i(t)]_{\pm} \rangle = R^{\pm}_{\sigma_b}\left(\frac{\nu_i - \langle r_i(t) \rangle}{\beta_b}\right).\end{aligned} \tag{12}$$

The transfer function for synaptic elements is given by $R_\sigma(\mu) = \frac{1}{2}\left(\mu + \mu \operatorname{erf}\left(\frac{\mu}{\sqrt{2}\sigma}\right) + \sqrt{\frac{2}{\pi}}\sigma e^{-\frac{\mu^2}{2\sigma^2}}\right)$, and the variance of the rate of elements is $\sigma_x^2 = \frac{\eta^2 \nu_i}{2\tau_{\text{Ca}}\beta_x^2}$. The parameter η is a correction factor, which accounts for the regularity of spike trains. In our case $\eta = \text{CV}$. Even if the mean number of free elements is zero, the noise will still drive the creation and deletion of elements with rate $\frac{\sigma_x}{\sqrt{2\pi}}$. Even if homeostatic control manages to drive all neurons to their target rates, the inherent calcium fluctuations and the associated uncertainty of firing rate inference will still induce random rewiring.

4.6 Mean-field approximation of population dynamics

We define population means for variables $x \in \{r, \phi, a, b\}$ and neuronal populations Y, Z as

$$\begin{aligned}x_Y(t) &= \frac{1}{N_Y}\sum_{i \in Y} x_i(t) \\ C_{YZ}(t) &= \frac{1}{N_Y N_Z}\sum_{i \in Y}\sum_{j \in Z} C_{ij}(t),\end{aligned}$$

where N_Y is the size of population Y. An individual neuron in population Y typically gets many inputs from every other neuronal population, which invites use of mean-field approximation due to the central limit theorem. The resulting currents aggregate to a Gaussian white noise process with mean and variances given as

$$\begin{aligned}\mu_Y(t) &= J\tau \sum_{Z \in \mathcal{E}} C_{YZ}(t) N_Z r_Z(t - D) - gJ\tau C_I r_I(t - D) + \tau J C_E \nu_{ext}, \\ \sigma_Y^2(t) &= J^2\tau \sum_{Z \in \mathcal{E}} C_{YZ}(t) N_Z r_Z(t - D) + g^2 J^2 \tau C_I r_I(t - D) + \tau J^2 C_E \nu_{ext}.\end{aligned}$$

The stationary firing rate of a leaky integrate-and-fire neuron driven by input with mean μ and variance σ^2 is [1]

$$r = f(\mu, \sigma) = \left(\tau_r + \tau_m \sqrt{\pi} \int_{\frac{V_r - \mu}{\sigma}}^{\frac{V_r - \theta}{\sigma}} e^{u^2}(1 + \operatorname{erf}(u))\,du\right)^{-1}.$$

Solving the time-dependent self-consistency problem for multiple interacting plastic populations is a challenging problem. We suggest here to use an adiabatic approximation, resorting to the fact that the firing rate dynamics is much faster than the plastic growth processes. Therefore, we employ a Wilson-Cowan type of the firing rate dynamics [27]

$$\tau_{\text{rate}} \dot{r}_Y(t) = -r_Y(t) + f(\mu_Y(t), \sigma_Y(t)). \tag{13}$$

The relaxation time is set to $\tau_{\text{rate}} < \tau_m$ to account for the fact that population response is generally much faster than the membrane potential dynamics [14]. The parameter τ_{rate} is the only free parameter in this model, but our

results do not depend on its exact value as long as $\tau_{\text{rate}} \leq \tau_m$. The heuristic described by Equation 13 results in a tractable and numerically stable system to be analyzed with standard dynamical system tools.

As the equation is linear, the average number of elements can be computed without approximation

$$\tau_{\text{Ca}}\dot{\phi}_Y(t) = r_Y(t) - \phi_Y(t). \tag{14}$$

As a consequence, the rate of element creation and deletion is also linear

$$\rho_{dY}(t) = \frac{1}{\beta_d}(\nu_Y - \phi_Y(t)) \qquad \rho_{aY}(t) = \frac{1}{\beta_a}(\nu_Y - \phi_Y(t)).$$

Finally we calculate the average connectivity

$$\dot{C}_{Y,Z}(t) = \frac{\rho'^{+}_{dY}(t)\rho'^{+}_{aZ}(t)}{\rho(t)} + C_{Y,Z}(t)\left(\frac{\rho^{-}_{dY}(t)}{k^i_Y(t)} + \frac{\rho^{-}_{aZ}(t)}{k^o_Y(t)}\right). \tag{15}$$

Here, $\rho^{\pm}_{dY}(t) = R_\sigma(\pm\rho^{\pm}_{dY}(t))$, $\rho^{\pm}_{aY}(t) = R_\sigma(\pm\rho^{\pm}_{aY}(t))$, and $\rho(t)$ is same as before, while the corrected rate for free elements is

$$\rho'^{+}_{aY}(t) = \frac{1}{\beta_d}(\nu_Y - \phi_Y(t)) + \sum_{Z\in\mathcal{E}} \frac{\rho^{-}_{dZ}(t)}{K^{in}_Z(t)} N_Z C_{\text{pop}_k,Y}(t)$$

$$\rho'^{+}_{dY}(t) = \frac{1}{\beta_a}(\nu_Y - \phi_Y(t)) + \sum_{Z\in\mathcal{E}} C_{YZ}(t) N_Z \frac{\rho^{-}_{ak}(t)}{K^{out}_Z(t)}.$$

4.7 Line attractor of the deterministic system

We represent the state of the network consisting of one static inhibitory and two plastic excitatory ensembles as a vector

$$\mathbf{y}(t) = (\phi_{E_1}(t), \phi_{E_2}(t), C_{E_1E_1}(t), C_{E_1E_2}(t), C_{E_2E_1}(t), C_{E_2E_2}(t), r_{E_1}(t), r_{E_2}(t), r_I(t))^T,$$

the components of which adhere to the calcium dynamics Equation 14, the connectivity dynamics Equation 15, and the activity dynamics Equation 13. The joint ODE system $\frac{d\mathbf{y}}{dt} = \mathbf{F}(\mathbf{y}, t)$ defines the vector field $\mathbf{F}$. We first explore the stationary states of the deterministic system ($\sigma_x = 0$), setting the left hand side of all ODEs to zero. In this case, calcium concentration and excitatory firing rates are fixed at their target values, and inhibitory firing rates r^*_I can be obtained using the self-consistency Equation 13. Stationary connectivity is calculated from the condition that the rates of creation and deletion of synaptic elements are zero. This implies that the numbers of free axonal and dendritic elements are zero, $\mathbf{a}^{\pm} = \mathbf{0}$ and $\mathbf{d}^{\pm} = \mathbf{0}$, which in turn implies that $\mathbf{a} = \mathbf{1}^T \cdot \mathbf{C}$ and $\mathbf{d} = \mathbf{C} \cdot \mathbf{1}$. The second condition is that all axonal elements are bonded with a dendritic element, and the total number of both types of elements are the same $|\mathbf{a}| = |\mathbf{d}|$.

Let us consider the case of two plastic excitatory ensembles E_1 and E_2 and one static inhibitory population I.

Using the parameter $x = C_{E_1E_1}$, the stationary state of the deterministic network is a line

$$\mathbf{l}(x) = \begin{bmatrix} \phi^*_{E1} \\ \phi^*_{E2} \\ C^*_{E_1E_1} \\ C^*_{E_1E_2} \\ C^*_{E_2E_1} \\ C^*_{E_2E_2} \\ r^*_{E1} \\ r^*_{E2} \\ r^*_I \end{bmatrix} = \begin{bmatrix} \nu \\ \nu \\ x \\ \frac{K^*_{E1}}{N_{E2}} - x\frac{N_{E1}}{N_{E2}} \\ \frac{K^*_{E1}}{N_{E2}} - x\frac{N_{E1}}{N_{E2}} \\ \left(\frac{K^*_{E2}}{N_{E2}} - \frac{N_{E1}}{N_{E2}}\frac{K^*_{E1}}{N_{E2}}\right) + x\left(\frac{N_{E1}}{N_{E2}}\right)^2 \\ \nu \\ \nu \\ r^*_I \end{bmatrix}. \tag{16}$$

Here, K^*_Y is the mean stationary in-degree, and we assume that the dendritic element growth factor β_d is less or equal to the axonal element growth factor β_a. The attractor is a line segment, as a consequence of linear conditions for element numbers and non-negativity of excitatory connections $C_{ij} \geq 0$. This solution can be easily generalized to a solution for individual connections of N_E excitation neurons, or for the case of n_E excitatory populations. The minimal invariant changes of the stationary connectivity matrix $\mathbf{C}$ that keep in-degree and out-degree conditions valid are of the type

$$\begin{pmatrix} \ddots & & & & \iddots \\ & 1 & \dots & -1 & \\ & \vdots & \ddots & \vdots & \\ & -1 & \dots & 1 & \\ \iddots & & & & \ddots \end{pmatrix},$$

where all missing entries are considered to be zero. This transformation defines a hyperplane section invariant space. The stationary connectivity can be solved as

$$|\mathbf{a}| = |\mathbf{d}| \tag{17}$$

$$\mathbf{C} = \begin{pmatrix} C_{11} & \cdots & C_{1(N_E-1)} & d_1 - \sum_{k=1}^{N_E-1} C_{1k} \\ \vdots & \ddots & \vdots & \vdots \\ C_{(N_E-1)1} & \cdots & C_{(N_E-1)(N_E-1)} & d_{N_E-1} - \sum_{k=1}^{N_E-1} C_{(N_E-1)k} \\ a_1 - \sum_{k=1}^{N_E-1} C_{k1} & \cdots & a_{N_E-1} - \sum_{k=1}^{N_E-1} C_{k(N_E-1)} & d_n - \sum_k^{N-1} a_k + \sum_{l=1,m=1}^{N_E-1} C_{lm} \end{pmatrix}$$

Note that we have put degree conditions in the place of the last raw and last column, but there is a permutation symmetry. The hyperplane for individual neurons has $N_E(N_E-3)+1$ dimensions, if there are no self-connections. In the case of n_E excitatory populations, the hyperplane has $n_E(n_E-2)+1$ dimensions.

4.8 Slow manifold and diffusion to the global fixed point

Now we calculate the stationary state for the stochastic system and assess the geometry and stability of the underlying phase space. In the case of finite noise, $\sigma_d > 0$, Equation 11 has an attractive fixed point, instead of a hyperplane attractor. The fixed point is given by

$$C^*_{i,j} = \frac{{\rho'_{d_i}}^+ {\rho'_{a_j}}^+}{\rho(\rho_{d_i}^- K_j^{\text{out}} + \rho_{a_j}^- K_j^{in})} K_i^{in} K_j^{\text{out}}. \tag{18}$$

Here, without loss of generality, we have assumed that the growth rate of dendritic elements is smaller or equal as compared to axonal elements. We obtain a normalized outer product of the indegree and outdegree vectors, respectively. In the case of identical dynamics for axonal and dendritic elements, and if all neurons have the same target rate $\nu_i = \nu$, we obtain the fixed point by plugging in the homogeneous solution

$$C^*_{i,j} = \frac{K^{\text{in}}}{N_E} = c. \tag{19}$$

This fixed point depends only on the indegree of neurons. For a two-population system, the fixed point is $\mathbf{y} = \mathbf{l}(\frac{K^{\text{in}}}{N_E})$, the most entropic configuration of the line segment attractor. This suggests a special importance for the relic of the line-attractor, which turns into a stochastic slow manifold through the presence of noise. The system relaxes along the direction of the slow manifold. Therefore, although rates of creation and deletion are the same around slow manifold, upon perturbation the system follows a fast trajectory off the slow manifold, and it relaxes slowly along the slow manifold towards the fixed point.

We now calculate the relaxation time for the three-population system to assess the persistence of a memory trace. To this end, we calculate the Jacobian $\mathcal{J} = \frac{\partial \mathbf{F}(\mathbf{y},t)}{\partial \mathbf{y}}\Big|_{\mathbf{y}=\mathbf{l}(x)}$ on the slow manifold, using a linearization of the vector field $\mathbf{F}$ (see Section 4.7). For the stochastic system, the Jacobian $\mathcal{J}(\mathbf{C}^*)$ about the global fixed point is

$$\mathcal{J} = \begin{bmatrix} -\frac{1}{\tau_{\text{Ca}}} & 0 & 0 & 0 & 0 & 0 & \frac{1}{\tau_{\text{Ca}}} & 0 & 0 \\ 0 & -\frac{1}{\tau_{\text{Ca}}} & 0 & 0 & 0 & 0 & 0 & \frac{1}{\tau_{\text{Ca}}} & 0 \\ J_{31} & J_{32} & J_{33} & J_{34} & J_{35} & J_{35} & 0 & 0 & 0 \\ J_{41} & J_{42} & J_{43} & J_{44} & J_{45} & J_{46} & 0 & 0 & 0 \\ J_{51} & J_{52} & J_{53} & J_{54} & J_{55} & J_{56} & 0 & 0 & 0 \\ J_{61} & J_{62} & J_{63} & J_{64} & J_{65} & J_{66} & 0 & 0 & 0 \\ 0 & 0 & J_{73} & J_{74} & 0 & 0 & J_{77} & J_{78} & J_{79} \\ 0 & 0 & 0 & 0 & J_{85} & J_{86} & J_{88} & J_{78} & J_{89} \\ 0 & 0 & 0 & 0 & 0 & 0 & J_{99} & J_{98} & J_{99} \end{bmatrix}. \tag{20}$$

The Jacobian has a block structure, which corresponds to calcium activity (black rectangle in Equation 20), connectivity $\mathcal{J}_c$ (blue rectangle) and spike activity $\mathcal{J}_r$ (red rectangle). The connectivity block around fixed point $\mathbf{y} = \mathbf{l}(c)$ is given by

$$\mathcal{J}_c = c0 \begin{bmatrix} -N_{E2}^2 & N_{E2}^2 & N_{E2}^2 & -N_{E2}^2 \\ N_{E1}N_{E2} & -N_{E1}N_{E2} & -N_{E1}N_{E2} & N_{E1}N_{E2} \\ N_{E1}N_{E2} & -N_{E1}N_{E2} & -N_{E1}N_{E2} & N_{E1}N_{E2} \\ -N_{E1}^2 & N_{E1}^2 & N_{E1}^2 & -N_{E1}^2 \end{bmatrix},$$

where $c_0 = \frac{\eta\sqrt{\frac{\nu}{\pi\tau_{\text{Ca}}}}}{2cN_E^3}\left(\frac{1}{\beta_a} + \frac{1}{\beta_b}\right)$. Jacobian entries responsible for interaction between connectivity variables and calcium activity variables are $-J_{42} = -J_{52} = J_{61} = \frac{N_{E1}}{N_E^2\beta_b}$, $J_{32} = -J_{41} = -J_{51} = \frac{N_{E2}}{N_E^2\beta_b}$, $J_{31} = -\frac{n_{E1}+2N_{E2}}{N_E^2\beta_b}$ and $J_{62} = -\frac{2N_{E1}+N_{E2}}{N_E^2\beta_b}$. The spike activity terms in the Jacobian are

$$\mathcal{J}_r = \frac{1}{\tau_{\text{rate}}} \begin{bmatrix} -1 + j_{EE}C_{E_1E_1}N_{E1} & j_{EE}C_{E_1E_2}N_{E2} & j_{EI}\epsilon N_I \\ j_{EE}C_{E_2E_1}N_{E1} & -1 + j_{EE}C_{E_2E_2}N_{E2} & j_{EI}\epsilon N_I \\ j_{IE}\epsilon N_{E1} & J_{IE}\epsilon N_{E1} & -1 + j_{II}\epsilon N_I \end{bmatrix}$$

Here we define the effective interaction of different neuron types neurons as excitatory-to-excitatory $j_{EE} = J\tau\frac{\partial f(\mu_E,\sigma_E)}{\partial \mu_E} + \frac{J^2\tau}{\sigma_E}\frac{\partial f(\mu_E,\sigma_E)}{\partial \sigma_E}$, inhibitory-to-excitatory $j_{EI} = -gJ\tau\frac{\partial f(\mu_E,\sigma_E)}{\partial \mu_E} + \frac{J^2\tau}{\sigma_E}\frac{\partial f(\mu_E,\sigma_E)}{\partial \sigma_E}$, excitatory-to-inhibitory $j_{IE} = J\tau\frac{\partial f(\mu_I,\sigma_I)}{\partial \mu_I} + \frac{J^2\tau}{\sigma_I}\frac{\partial f(\mu_I,\sigma_I)}{\partial \sigma_I}$ and inhibitory-to-inhibitory neurons as $j_{II} = -gJ\tau\frac{\partial f(\mu_I,\sigma_I)}{\partial \mu_I} + \frac{g^2J^2\tau}{\sigma_I}\frac{\partial f(\mu_I,\sigma_I)}{\partial \sigma_I}$. The Jacobian elements which are responsible for influence of connectivity change to rates are $J_{73} = \frac{1}{\tau_{\text{rate}}} j_{EE} N_{E1} r_{E1}$, $J_{74} = \frac{1}{\tau_{\text{rate}}} j_{EE} N_{E2} r_{E2}$, $J_{85} = \frac{1}{\tau_{\text{rate}}} j_{EE} N_{E1} r_{E1}$ and $J_{86} = \frac{1}{\tau_{\text{rate}}} j_{EE} N_{E2} r_2$. These terms are the largest in the Jacobian, but since connectivity changes only through a change of calcium, they will not play an essential role for long-term stability.

We exploit the block structure of the Jacobian $\mathcal{J}$ to separate between connectivity variables, the fast firing rate and calcium variables. We can solve the connectivity eigenproblem analytically,

$$\boldsymbol{\lambda}_0^0 = \begin{bmatrix} 0 \\ 0 \\ 1 \\ 1 \\ 1 \\ 1 \\ 0 \\ 0 \\ 0 \end{bmatrix} \quad \boldsymbol{\lambda}_0^1 = \begin{bmatrix} 0 \\ 0 \\ 1 \\ 1 \\ -\frac{N_{E1}}{N_{E2}} \\ -\frac{N_{E1}}{N_{E2}} \\ 0 \\ 0 \\ 0 \end{bmatrix} \quad \boldsymbol{\lambda}_0^2 = \begin{bmatrix} 0 \\ 0 \\ 1 \\ -\frac{N_{E1}}{N_{E2}} \\ 1 \\ -\frac{N_{E1}}{N_{E2}} \\ 0 \\ 0 \\ 0 \end{bmatrix} \quad \boldsymbol{\lambda}_1 = \begin{bmatrix} 0 \\ 0 \\ 1 \\ -\frac{N_{E1}}{N_{E2}} \\ -\frac{N_{E1}}{N_{E2}} \\ \left(\frac{N_{E1}}{N_{E2}}\right)^2 \\ 0 \\ 0 \\ 0 \end{bmatrix}, \tag{21}$$

with eigenvalues $\lambda_0 = 0$ and $\lambda_1 = -\frac{R_{\sigma_a}(0)+R_{\sigma_b}(0)}{cN_E}$.

The persistence of a memory trace in the system with noise is essentially determined by the diffusion to the global fixed point. In fact, the line attractor of the noiseless system turns into a slow manifold of the noisy system. The eigenvalue λ_0 is degenerate, and the three-dimensional invariant space defines the central manifold of the connectivity subsystem. The eigenvalue λ_1 is also an eigenvalue of the full Jacobian $\mathcal{J}$ and it represents the slowest time scale of the system in the direction of the slow manifold. It is easy to check that $\partial_x \mathbf{l}(x) = \boldsymbol{\lambda}_1$. This means that the noiseless line attractor is exactly corresponding to the slow manifold of the system. The other eigenvectors have components orthogonal to the slow manifold. Those are dominated by fast variables, and they relax quickly. As a result, the relaxation dynamics is dominated by the eigenvalue λ_1, and the relaxation time of the system under consideration is

$$\tau_{\text{diffusion}} = \sqrt{\frac{4\pi\tau_{\text{Ca}}}{\eta^2\nu}}\frac{N_E c}{\frac{1}{\beta_d}+\frac{1}{\beta_a}}.$$

For the default parameters used here, its value is around 5 000 s, fully in accordance with numerical simulations.

A quantitative measure for the volatility of network structure used in experiments is the turnover ratio (TOR) of dendritic spines [41]. It is defined as $\text{TOR} = \frac{\Delta N_{\text{new}} + \Delta N_{\text{deleted}}}{2N_{\text{spines}}}$, where the changes ΔN_{new} and $\Delta N_{\text{deleted}}$ are typically measured per day. For the case when the network plasticity is selectively driven by diffusion, this quantity corresponds to the eigenvalue λ_1, corresponding to a value around 18 % per day for standard parameters.

4.9 Linear stability analysis

Numerical exploration of the eigenvalues show that for our system there is linear stability for a wide parameter range. However this system can produce damped oscillations, which may cause problems. We use a reduced

system of only one plastic excitatory population and one static inhibitory population to analyze the influence of the calcium time constant and element growth. This gives rise to the Jacobian

$$\mathcal{J}_1 = \begin{bmatrix} -\frac{1}{\tau_{\mathrm{Ca}}} & 0 & \frac{1}{\tau_{\mathrm{Ca}}} & 0 \\ -\frac{1}{NE\beta_d} & 0 & 0 & 0 \\ 0 & \frac{1}{\tau_{\mathrm{rate}}} j_{EE} c N_E & -\frac{1}{\tau_{\mathrm{rate}}} + \frac{1}{\tau_{\mathrm{rate}}} j_{EE} c N_E & \frac{1}{\tau_{\mathrm{rate}}} j_{EI} \epsilon N_I \\ 0 & 0 & \frac{1}{\tau_{\mathrm{rate}}} J_{IE} \epsilon N_E & -\frac{1}{\tau_{\mathrm{rate}}} + \frac{1}{\tau_{\mathrm{rate}}} j_{II} \epsilon N_I \end{bmatrix}.$$

The eigenvalues of $\mathcal{J}_1$ have been reduced to radicals using *Mathematica* 12.0, and the complex conjugated eigenvalues $\lambda_{3/4}$ responsible for oscillations are plotted in Figure 6.

Although there is linear stability around the global fixed points for wide parameter range, the same is not the true for all points along the line attractor. The connectivity eigenvalue λ_1 is constant on the slow manifold, but if one population presents large recurrent connectivity, spike activity jumps to a persistent high activity state. We can track this instability in the Jacobian $\mathcal{J}(x)$ along the line attractor $l(x)$. As the recurrent connectivity of the first ensemble $E1$ is increased, one of the eigenvalues becomes positive, and its corresponding eigenvector makes the biggest contributions in the direction of spike activity r_{E1} and r_{E2}. Here we use this fact and use the reduced Jacobian

$$\mathcal{J}_r = \begin{bmatrix} \frac{\partial F_7(\mathbf{y},t)}{\partial r_{E1}} & \frac{\partial F_7(\mathbf{y},t)}{\partial r_{E2}} \\ \frac{\partial F_8(\mathbf{y},t)}{\partial r_{E1}} & \frac{\partial F_8(\mathbf{y},t)}{\partial r_{E2}} \end{bmatrix} = \frac{1}{\tau_{\mathrm{rate}}} \begin{bmatrix} -1 + j_{EE} C_{E_1E_1} N_{E1} & j_{EE} C_{E_1E_2} N_{E2} \\ j_{EE} C_{E_2E_1} N_{E1} & -1 + j_{EE} C_{E_2E_2} N_{E2} \end{bmatrix}$$

to find the approximate position of this transition on the line attractor. The spiking activity becomes unstable, when the real part of the second eigenvalue λ_2^r becomes positive, and at this point the determinant of the Jacobian changes its sign (since both eigenvalues are real). We can use this criterion to determine when the system loses linear stability, leading to the critical value c_{crit} of connectivity $C_{E_1E_1}$

$$c_{\mathrm{crit}} = \epsilon \left(1 + \frac{N_{E2}}{N_{E1} j_E}\right), \tag{22}$$

where j_E is a dimension-less measure of effective excitatory excitability $j_E = \epsilon N_E j_{EE}$. The value c_{crit} is the upper bound of full stability, but the system loses stability even below this value, as discussed in our results.

4.10 Network simulations

All simulations have been performed using the neural network simulator NEST 2.16.0 [28].

4.10.1 Grown networks

All numerical stimulation experiments start from grown networks. To this end, we initialize a network with random connections to and from inhibitory neurons and no excitatory-to-excitatory connections, whatsoever. The latter are then grown under the control of homeostatic structural plasticity. The controlled variable is the firing rate of excitatory neurons, the target rate is set to $\nu = 8\,\mathrm{Hz}$ for all neurons. During this initial growth period, excitatory neurons receive external Poisson input of rate $\nu_{\mathrm{ext}} = 15\,\mathrm{kHz}$. After a long-enough growth time t_{growth}, the network structure has reached its equilibrium and all neurons fire at their target rate, apart from small fluctuations.

4.10.2 Conditioning paradigm

Non-overlapping neuronal ensembles comprising 10 % of all excitatory neurons each are selected and labeled US, C1 and C2. Non-plastic connections of weight $J_E = 0.1\,\mathrm{mV}$ are created from all neurons labeled US to a readout neuron, which has the same properties as all the other neurons in the network. Stimulation is specific for a certain group of neurons. A stimulation cycle consists of an increased external input rate of $1.4\,\nu_{\mathrm{ext}}$ for a period of 2 s, followed by a relaxation period of 48 s, during which the external input is set back to ν_{ext}.

The whole protocol consists of 5 different episodes: growth, baseline, encoding, decay and retrieval. During "baseline" each of the 3 groups is stimulated alone in the order US, C1, C2. The "encoding" episode consists of 6 stimulation cycles. In 3 out of the 6 cycles, C2 is stimulated alone. In the other 3 cycles, neurons from both US and C1 are stimulated at the same time. The "decay" episode lasts 100 s, during which no stimulation beyond ν_{ext} is applied. During "retrieval", there are 2 stimulation cycles, C1 alone is followed by C2 alone. Connectivity is recorded every 1 s. In this protocol, plasticity is always on, and all measurements are performed in the plastic network. Growth time is $t_{\mathrm{growth}} = 100\,\mathrm{s}$, the remaining parameters are $\beta_d = \beta_a = 0.4$, $\tau_{\mathrm{Ca}} = 1\,\mathrm{s}$, $\Delta T_s = 10\,\mathrm{ms}$.

4.10.3 Repeated stimulation

Starting from a grown network, a random neuronal ensemble comprising 10 % of all excitatory neurons in the network is repeatedly stimulated for 8 cycles. Here, a stimulation cycle consists of a stimulation period of 150 s, during which the external input to the ensemble neurons is increased to $1.05\,\nu_{\mathrm{ext}}$. It is followed by a relaxation period of 150 s, during which the external input is set back to ν_{ext}. During stimulation, the connectivity is recorded every 15 s. After encoding the engram, plasticity is turned off, and all measurements are now performed in a non-plastic network. Growth time is $t_{\mathrm{growth}} = 500\,\mathrm{s}$, the remaining parameters are $\beta_d = \beta_a = 2$, $\tau_{\mathrm{Ca}} = 10\,\mathrm{s}$, $\Delta T_s = 100\,\mathrm{ms}$.

4.10.4 Readout neuron

Two non-overlapping ensembles comprising 10 % of all excitatory neurons each are randomly selected and labeled A_1 and A_2. Starting from a grown network, A_1 is stimulated twice. During each stimulation cycle, the external input to stimulated neurons is increased to $1.1\,\nu_{\mathrm{ext}}$ for a time period of 150 s. This is followed by a relaxation period of 150 s, during which the external input is set back to ν_{ext}. After a pause of 100 s, A_2 is stimulated once using otherwise the same protocol. Growth time is $t_{\mathrm{growth}} = 500\,\mathrm{s}$, the remaining parameters are $\beta_d = \beta_a = 2$, $\tau_{\mathrm{Ca}} = 10\,\mathrm{s}$, $\Delta T_s = 100\,\mathrm{ms}$.

After the encoding of engrams, plasticity is turned off. A readout neuron is added to the network, which has the same properties as all other neurons in the network. Non-plastic connections of weight $J_E = 0.1\,\mathrm{mV}$ are created from a random sample comprising 9 % of all excitatory and 9 % of all inhibitory neurons in the network. Two new non-overlapping ensembles comprising 10 % of all excitatory neurons each are selected as random patterns A_3 and A_4. Neurons in the network are stimulated in the order A_3, A_2, A_1, A_4. During each stimulation cycle, the external input to neurons in the corresponding group is increased to $1.1\,\nu_{\mathrm{ext}}$ for a period of 1 s duration. This is followed by a non-stimulation period of 4 s, during which external input rate is set back to ν_{ext}.

4.10.5 Formation and decay of engrams

Starting from a grown network, a subgroup comprising 10 % of all excitatory neurons is randomly selected and stimulated for 150 s, followed by a prolonged relaxation period of 5 500 s. During stimulation, the external input to stimulated neurons is increased to $1.1\,\nu_{\text{ext}}$. For all simulations, $\beta_d = \beta_a = 2$, $\Delta T_s = 100$ ms.

The simulations to demonstrate how τ_{decay} changes with τ_{Ca} were performed with a target rate $\nu = 8$ Hz and $\tau_{\text{Ca}} = 2, 4, 8, 16, 32$ s. The simulations showing how τ_{decay} changes with ν were performed with $\tau_{\text{Ca}} = 10$ s and $\nu = 2, 4, 8, 16, 32$ Hz. In the simulations performed with $\nu = 2, 4$ Hz, $\tau_{\text{growth}} = 5\,000$ s, neurons are stimulated for 1 500 s, and the relaxation period is 26 000 s. The parameter τ_{decay} is estimated from simulated time series by performing a least-squares fit of an exponential function to the connectivity values during the decay period, and extracting the fitted time constant.

4.10.6 Linear stability

Starting from a grown network, a subgroup comprising 10 % of all excitatory neurons is randomly selected and stimulated for a time period t_{stim}. During stimulation, the external input to stimulated neurons is increased to $1.1\,\nu_{\text{ext}}$. Stimulation is followed by a period of duration t_{relax}, during which the external input is set back to ν_{ext} and the connectivity relaxes back to a new equilibrium. The parameters used are for non-oscillatory regime: $t_{\text{growth}} = t_{\text{stim}} = t_{\text{relax}} = 800$ s, $\beta_d = \beta_a = 2$, $\tau_{\text{Ca}} = 5$ s, $\Delta T_s = 1$ ms; for the weakly oscillatory regime: $t_{\text{growth}} = t_{\text{stim}} = t_{\text{relax}} = 400$ s, $\beta_d = \beta_a = 0.2$, $\tau_{\text{Ca}} = 20$ s, $\Delta T_s = 0.2$ ms; and for the strongly oscillatory regime: $t_{\text{growth}} = t_{\text{stim}} = t_{\text{relax}} = 200$ s, $\beta_d = \beta_a = 0.03$, $\tau_{\text{Ca}} = 10$ s, $\Delta T_s = 0.2$ ms.

4.10.7 Non-Linear stability

Starting from a grown network, a subgroup comprising 10% of all excitatory neurons is randomly selected and stimulated for 200 s. During stimulation, the external input rate to stimulated neurons is increased to $1.25\,\nu_{\text{ext}}$. Stimulation is followed by a relaxation time in which external input rate is set back to ν_{ext}. Growth time $t_{\text{growth}} = 500$ s, $\beta_d = \beta_a = 2$, $\tau_{\text{Ca}} = 10$ s, $\Delta T_s = 0.1$ ms. During and after stimulation, connectivity is recorded every 5 s.

4.10.8 Overlap measure

The similarity between network activity during stimulation, spontaneous and evoked responses is measured by the corresponding overlaps [15] defined as

$$m^{\mu} = [Na(1-a)]^{-1} \sum_i (\xi_i^{\mu} - a) s_i(t). \tag{23}$$

The pattern ξ^{μ} is a vector of dimension N. Each entry ξ_i^{μ} is a binary variable indicating whether or not neuron i is stimulated by pattern ξ^{μ}, and it has a mean value of $a = \langle \xi_i^{\mu} \rangle_i$. The activity vector $s_i(t)$ is also composed of binary variables, which indicate whether or not neuron i is active in a given time bin. In all figures, the bin size used for calculating overlaps is 10 ms.

4.10.9 Population firing rate

In Figure 3B, the population response of excitatory neurons is estimated for different connectivity values using a mean-field rate model [1]. We consider a model with three populations, two of which are excitatory (E_1 comprises 10 % and E_2 comprises 90 % of all $N_E = 10\,000$ excitatory neurons), and one is inhibitory with $N_I = 2\,500$ neurons. All connectivities involving inhibitory neurons are fixed and set to $\epsilon = 0.1$. For the excitatory-to-excitatory connections, we systematically vary the connectivity within the E_1 population ($C_{E_1E_1}$), and calculate the other values to achieve a constant excitatory in-degree of ϵN_E. All other parameters used are unchanged. For the different values of $C_{E_1E_1}$ we calculate the population rate of excitatory neurons for E_1 receiving a larger external input of $1.05\,\nu_{\text{ext}}$ as compared to the E_2 and I populations ($\nu_{\text{ext}} = 15\,\text{kHz}$).

4.10.10 Pattern completion

To address pattern completion, we employ the non-plastic network after engram encoding (see 4.10.3). Different fractions of the neurons belonging to the engram are stimulated for 10 s, and we calculate the overlap averaged over the stimulation time $\langle m^{E_1} \rangle$. For each fraction of stimulated neurons, 50 different simulations are run, during which a different subsample of the engram neurons is stimulated.

Table 1: List of symbols

Symbol	Description
$\phi(t)$	Calcium trace
τ_{Ca}	Calcium time constant
$S(t)$	Spike train
$r(t)$	Instantaneous firing rate
ν	Target rate
$a(t)$	Number of axonal elements
$d(t)$	Number of dendritic elements
β_d	Dendritic growth parameter
β_a	Axonal growth parameter
$C_{ij}(t)$	Number of synaptic connections from neuron j (presynaptic) to neuron i (postsynaptic)
E	Excitatory neurons
E_1	Stimulated excitatory neurons
E_2	Non-stimulated excitatory neurons
I	Inhibitory neurons
τ_{drift}	Effective time constant of encoding
$\tau_{\mathrm{diffusion}}$	Effective time constant of forgetting
$m^x(t)$	Overlap of network activity with pattern x
τ_{rate}	Relaxation time of rate dynamics

5 Acknowledgements

Supported by Erasmus Mundus / EuroSPIN, DFG (grant EXC 1086) and Carl Zeiss Foundation. The HPC facilities are funded by the state of Baden-Württemberg through bwHPC and DFG grant INST 39/963-1 FUGG. We thank Sandra Diaz-Pier and Mikaël Naveau from the Research Center Jülich for support on new features of NEST, and Uwe Grauer from the Bernstein Center Freiburg as well as Bernd Wiebelt and Michael Janczyk from the Freiburg University Computing Center for their assistance with HPC applications.

References

[1] Nicolas Brunel. "Dynamics of Sparsely Connected Networks of Excitatory and Inhibitory Spiking Neurons". en. In: *Journal of Computational Neuroscience* 8.3 (May 2000), pp. 183–208. DOI: 10.1023/A:1008925309027. URL: https://www.ncbi.nlm.nih.gov/pubmed/10809012.

[2] Markus Butz and Arjen van Ooyen. "A simple rule for dendritic spine and axonal bouton formation can account for cortical reorganization after focal retinal lesions." In: *PLoS computational biology* 9.10 (Jan. 2013), e1003259. ISSN: 1553-7358. DOI: 10.1371/journal.pcbi.1003259. URL: http://journals.plos.org/ploscompbiol/article?id=10.1371/journal.pcbi.1003259.

[3] Markus Butz, Ines D Steenbuck, and Arjen van Ooyen. "Homeostatic structural plasticity can account for topology changes following deafferentation and focal stroke." In: *Frontiers in Neuroanatomy* 8 (Jan. 2014), p. 115. ISSN: 1662-5129. DOI: 10.3389/fnana.2014.00115. URL: https://www.ncbi.nlm.nih.gov/pubmed/25360087.

[4] Markus Butz, Ines D Steenbuck, and Arjen van Ooyen. "Homeostatic structural plasticity increases the efficiency of small-world networks." In: *Frontiers in Synaptic Neuroscience* 6.April (Jan. 2014), p. 7. ISSN: 1663-3563. DOI: 10.3389/fnsyn.2014.00007. URL: https://www.ncbi.nlm.nih.gov/pubmed/24744727.

[5] Markus Butz, Arjen Van Ooyen, and Florentin Wörgötter. "A model for cortical rewiring following deafferentation and focal stroke." In: *Frontiers in Computational Neuroscience* 3.August (Jan. 2009), p. 10. ISSN: 1662-5188. DOI: 10.3389/neuro.10.010.2009. URL: https://www.ncbi.nlm.nih.gov/pubmed/19680468.

[6] Markus Butz et al. "A theoretical network model to analyse neurogenesis and synaptogenesis in the dentate gyrus". In: *Neural Networks* 19.10 (2006), pp. 1490–1505. ISSN: 08936080. DOI: 10.1016/j.neunet.2006.07.007. URL: https://www.ncbi.nlm.nih.gov/pubmed/17014989.

[7] Markus Butz et al. "Inverse relationship between adult hippocampal cell proliferation and synaptic rewiring in the dentate gyrus". In: *Hippocampus* 18.9 (Jan. 2008), pp. 879–898. ISSN: 1098-1063. DOI: 10.1002/hipo.20445. URL: https://www.ncbi.nlm.nih.gov/pubmed/18481284.

[8] György Buzsáki and Kenji Mizuseki. "The log-dynamic brain: how skewed distributions affect network operations." In: *Nature Reviews Neuroscience* 15.4 (Apr. 2014), pp. 264–278. ISSN: 1471-0048. DOI: 10.1038/nrn3687. URL: http://www.ncbi.nlm.nih.gov/pubmed/24569488.

[9] Sandra Diaz-Pier et al. "Automatic Generation of Connectivity for Large-Scale Neuronal Network Models through Structural Plasticity". English. In: *Frontiers in Neuroanatomy* 10 (May 2016). ISSN: 1662-5129. DOI: 10.3389/fnana.2016.00057. URL: https://www.ncbi.nlm.nih.gov/pubmed/27303272.

[10] Michael Jan Fauth and Mark CW van Rossum. "Self-organized reactivation maintains and reinforces memories despite synaptic turnover". In: *eLife* 8 (May 2019). DOI: 10.7554/eLife.43717. URL: http://www.ncbi.nlm.nih.gov/pubmed/31074745.

[11] Michael Fauth, Florentin Wörgötter, and Christian Tetzlaff. "Formation and Maintenance of Robust Long-Term Information Storage in the Presence of Synaptic Turnover". In: *PLOS Computational Biology* 11.12 (Dec. 2015). Ed. by Jeff Beck, e1004684. ISSN: 1553-7358. DOI: 10.1371/journal.pcbi.1004684. URL: http://www.ncbi.nlm.nih.gov/pubmed/26713858.

[12] Júlia V. Gallinaro and Stefan Rotter. "Associative properties of structural plasticity based on firing rate homeostasis in recurrent neuronal networks". In: *Scientific Reports* 8.1 (Dec. 2018), p. 3754. DOI: 10.1038/s41598-018-22077-3. URL: http://www.ncbi.nlm.nih.gov/pubmed/29491474.

[13] Samuel J. Gershman et al. "The computational nature of memory modification". In: *eLife* 6 (Mar. 2017). ISSN: 2050084X. DOI: 10.7554/eLife.23763.

[14] Wulfram Gerstner. "Population dynamics of spiking neurons: Fast transients, asynchronous states, and locking". In: *Neural Computation* 12.1 (Mar. 2000), pp. 43–89. ISSN: 08997667. DOI: 10.1162/089976600300015899. URL: https://www.ncbi.nlm.nih.gov/pubmed/10636933.

[15] Wulfram Gerstner et al. *Neuronal dynamics: From single neurons to networks and models of cognition*. Cambridge University Press, 2014.

[16] Benjamin F. Grewe and Fritjof Helmchen. "High-speed two-photon calcium imaging of neuronal population activity using acousto-optic deflectors". In: *Cold Spring Harbor Protocols* 2014.6 (June 2014), pp. 618–629. ISSN: 15596095. DOI: 10.1101/pdb.prot081778. URL: http://www.ncbi.nlm.nih.gov/pubmed/24890212.

[17] Benjamin F. Grewe et al. "High-speed in vivo calcium imaging reveals neuronal network activity with near-millisecond precision". In: *Nature Methods* 7.5 (May 2010), pp. 399–405. ISSN: 15487091. DOI: 10.1038/nmeth.1453.

[18] Moritz Helias et al. "Structural plasticity controlled by calcium based correlation detection". In: *Frontiers in Computational Neuroscience* 2.DEC (Dec. 2008). ISSN: 16625188. DOI: 10.3389/neuro.10.007.2008.

[19] Keith B Hengen et al. "Neuronal Firing Rate Homeostasis Is Inhibited by Sleep and Promoted by Wake". In: *Cell* 165.1 (2016), pp. 180–191. ISSN: 00928674. DOI: 10.1016/j.cell.2016.01.046. URL: https://www.ncbi.nlm.nih.gov/pubmed/26997481.

[20] Sonja B Hofer et al. "Differential connectivity and response dynamics of excitatory and inhibitory neurons in visual cortex". In: *Nature Neuroscience* 14.8 (Aug. 2011), pp. 1045–1052. DOI: 10.1038/nn.2876. URL: http://www.ncbi.nlm.nih.gov/pubmed/21765421.

[21] Anthony J.G.D. Holtmaat et al. "Transient and persistent dendritic spines in the neocortex in vivo". In: *Neuron* (2005). ISSN: 08966273. DOI: 10.1016/j.neuron.2005.01.003.

[22] Anthony Holtmaat and Karel Svoboda. "Experience-dependent structural synaptic plasticity in the mammalian brain." In: *Nature Reviews Neuroscience* 10.9 (Sept. 2009), pp. 647–58. ISSN: 1471-0048. DOI: 10.1038/nrn2699. URL: http://dx.doi.org/10.1038/nrn2699.

[23] Sheena A. Josselyn and Paul W. Frankland. "Memory Allocation: Mechanisms and Function". In: *Annual Review of Neuroscience* 41.1 (July 2018), pp. 389–413. DOI: 10.1146/annurev-neuro-080317-061956. URL: http://www.ncbi.nlm.nih.gov/pubmed/29709212.

[24] Sheena A. Josselyn, Stefan Köhler, and Paul W. Frankland. "Finding the engram". In: *Nature Reviews Neuroscience* 16.9 (Aug. 2015), pp. 521–534. ISSN: 1471-003X. DOI: 10.1038/nrn4000. URL: http://www.nature.com/doifinder/10.1038/nrn4000.

[25] Tara Keck et al. "Integrating Hebbian and homeostatic plasticity: the current state of the field and future research directions". In: *Philosophical Transactions of the Royal Society B* 372.1715 (Mar. 2017), p. 20160158. ISSN: 0962-8436. DOI: 10.1098/rstb.2016.0158. URL: http://rstb.royalsocietypublishing.org/lookup/doi/10.1098/rstb.2016.0158.

[26] Birgit Kriener et al. "Correlations and population dynamics in cortical networks". en. In: *Neural computation* 20.9 (Oct. 2008), pp. 2185–2226. ISSN: 0899-7667. DOI: 10.1162/neco.2008.02-07-474. URL: http://www.mitpressjournals.org/doi/abs/10.1162/neco.2008.02-07-474#.VRp5N8tdTyw.

[27] Erwan Ledoux and Nicolas Brunel. "Dynamics of networks of excitatory and inhibitory neurons in response to time-dependent inputs". In: *Frontiers in Computational Neuroscience* 5 (May 2011). ISSN: 16625188. DOI: 10.3389/fncom.2011.00025.

[28] Charl Linssen et al. "NEST 2.16.0". In: (Aug. 2018). DOI: 10.5281/ZENODO.1400175. URL: https://zenodo.org/record/1400175#.XWPrKZyxWVM.

[29] Ashok Litwin-Kumar and Brent Doiron. "Slow dynamics and high variability in balanced cortical networks with clustered connections". In: *Nature Neuroscience* 15.11 (Nov. 2012), pp. 1498–1505. DOI: 10.1038/nn.3220. URL: http://www.ncbi.nlm.nih.gov/pubmed/23001062.

[30] Ashok Litwin-Kumar and Brent Doiron. "Formation and maintenance of neuronal assemblies through synaptic plasticity". In: *Nature Communications* 5 (Nov. 2014), p. 5319. DOI: 10.1038/ncomms6319. URL: http://www.ncbi.nlm.nih.gov/pubmed/25395015.

[31] Yonatan Loewenstein, Uri Yanover, and Simon Rumpel. "Predicting the dynamics of network connectivity in the neocortex". In: *Journal of Neuroscience* 35.36 (Sept. 2015), pp. 12535–12544. ISSN: 15292401. DOI: 10.1523/JNEUROSCI.2917-14.2015.

[32] Han Lu, Júlia V. Gallinaro, and Stefan Rotter. "Network remodeling induced by transcranial brain stimulation: A computational model of tDCS-triggered cell assembly formation". In: *Network Neuroscience* (May 2019), pp. 1–21. DOI: 10.1162/netn{_}a{_}00097. URL: https://www.mitpressjournals.org/doi/abs/10.1162/netn_a_00097.

[33] Gianluigi Mongillo, Simon Rumpel, and Yonatan Loewenstein. *Intrinsic volatility of synaptic connections — a challenge to the synaptic trace theory of memory*. 2017. DOI: 10.1016/j.conb.2017.06.006.

[34] Karim Nader, Glenn E. Schafe, and Joseph E. Le Doux. "Fear memories require protein synthesis in the amygdala for reconsolidation after retrieval". In: *Nature* 406.6797 (Aug. 2000), pp. 722–726. DOI: 10.1038/35021052. URL: http://www.ncbi.nlm.nih.gov/pubmed/10963596.

[35] Martin P. Nawrot et al. "Measurement of variability dynamics in cortical spike trains". In: *Journal of Neuroscience Methods* 169.2 (Apr. 2008), pp. 374–390. ISSN: 01650270. DOI: 10.1016/j.jneumeth.2007.10.013. URL: https://www.ncbi.nlm.nih.gov/pubmed/18155774.

[36] Helen E. Scharfman. *The neurobiology of epilepsy*. July 2007. DOI: 10.1007/s11910-007-0053-z.

[37] Richard Wolfgang Semon. *The mneme*. London: Allen & Unwin, 1921. URL: https://archive.org/stream/cu31924100387210#page/n31/mode/2up.

[38] Mark G. Stokes. *'Activity-silent' working memory in prefrontal cortex: A dynamic coding framework*. July 2015. DOI: 10.1016/j.tics.2015.05.004.

[39] Christian Tetzlaff et al. "Self-Organized Criticality in Developing Neuronal Networks". In: *PLOS Computational Biology* 6.12 (Dec. 2010). Ed. by Karl J. Friston, e1001013. ISSN: 1553-7358. DOI: 10.1371/journal.pcbi.1001013. URL: https://www.ncbi.nlm.nih.gov/pubmed/21152008.

[40] Alejandro Torrado Pacheco et al. "Rapid and active stabilization of visual cortical firing rates across light–dark transitions". In: *Proceedings of the National Academy of Sciences* (July 2019), p. 201906595. ISSN: 0027-8424. DOI: 10.1073/pnas.1906595116.

[41] Joshua T Trachtenberg et al. "Long-term in vivo imaging of experience-dependent synaptic plasticity in adult cortex." In: *Nature* 420.6917 (2002), pp. 788–794. DOI: 10.1038/nature01273.

[42] Henry C. (Henry Clavering) Tuckwell. *Introduction to theoretical neurobiology*. Cambridge University Press, 1988. ISBN: 0521350964.

[43] Gina Turrigiano. "Homeostatic synaptic plasticity: local and global mechanisms for stabilizing neuronal function." In: *Cold Spring Harbor perspectives in biology* 4.1 (Jan. 2012), a005736. ISSN: 1943-0264. DOI: 10.1101/cshperspect.a005736. URL: https://www.ncbi.nlm.nih.gov/pubmed/22086977.

[44] Gina G. Turrigiano and Sacha B. Nelson. *Homeostatic plasticity in the developing nervous system*. 2004. DOI: 10.1038/nrn1327.

[45] Adelaide P. Yiu et al. "Neurons Are Recruited to a Memory Trace Based on Relative Neuronal Excitability Immediately before Training". In: *Neuron* 83.3 (Aug. 2014), pp. 722–735. ISSN: 10974199. DOI: 10.1016/j.neuron.2014.07.017. URL: https://www.ncbi.nlm.nih.gov/pubmed/25102562.

[46] Friedemann Zenke, Everton J Agnes, and Wulfram Gerstner. "Diverse synaptic plasticity mechanisms orchestrated to form and retrieve memories in spiking neural networks". en. In: *Nature Communications* 6 (Jan. 2015). ISSN: 2041-1723. DOI: 10.1038/ncomms7922. URL: https://www.ncbi.nlm.nih.gov/pubmed/25897632.

[47] Friedemann Zenke and Wulfram Gerstner. "Hebbian plasticity requires compensatory processes on multiple timescales". In: *Philosophical Transactions of the Royal Society B* 372.1715 (Mar. 2017), p. 20160259. ISSN: 0962-8436. DOI: 10.1098/rstb.2016.0259. URL: https://www.ncbi.nlm.nih.gov/pubmed/28093557.

[48] Yu Zhou et al. "CREB regulates excitability and the allocation of memory to subsets of neurons in the amygdala". In: *Nature Neuroscience* 12.11 (Nov. 2009), pp. 1438–1443. ISSN: 10976256. DOI: 10.1038/nn.2405. URL: https://www.ncbi.nlm.nih.gov/pubmed/19783993.

[49] Yaniv Ziv et al. "Long-term dynamics of CA1 hippocampal place codes". In: *Nature Neuroscience* 16.3 (Mar. 2013), pp. 264–266. DOI: 10.1038/nn.3329. URL: http://www.ncbi.nlm.nih.gov/pubmed/23396101.

[50] Yi Zuo et al. "Development of long-term dendritic spine stability in diverse regions of cerebral cortex". In: *Neuron* 46.2 (Apr. 2005), pp. 181–189. ISSN: 08966273. DOI: 10.1016/j.neuron.2005.04.001.